

1 **Tobramycin-induced secretion of *P. aeruginosa* 5' tRNA-fMet halves suppresses lung**
2 **inflammation via AGO2 gene silencing**

3 Zhongyou Li¹, Katja Koeppen¹, Alix Ashare^{1,2}, Deborah A. Hogan¹, Scott A. Gerber³, and Bruce
4 A. Stanton^{1*}

5 ¹Department of Microbiology and Immunology, Geisel School of Medicine at Dartmouth, Hanover,
6 NH, USA

7 ²Pulmonary and Critical Care Medicine, Dartmouth-Hitchcock Medical Center, Lebanon, NH,
8 USA

9 ³Norris Cotton Cancer Center, Geisel School of Medicine at Dartmouth, Lebanon, NH, USA

10

11 **Corresponding author:**

12 Bruce A. Stanton, Ph.D.

13 Department of Microbiology and Immunology

14 Geisel School of Medicine at Dartmouth

15 520 Renssen

16 Hanover NH 03755

17 Phone: 603-650-1775

18 Email: Bruce.A.Stanton@dartmouth.edu

19 **Running title: Tobramycin suppresses inflammation via tRNA halves**

20 **Keywords:** cystic fibrosis, tobramycin, outer membrane vesicles, tRNA halves, anti-
21 inflammatory

22 **The authors have declared that no conflict of interest exists.**

23 **Abstract**

24 Although inhaled tobramycin increases lung function in people with cystic fibrosis (pwCF), the
25 density of *P. aeruginosa* in the lungs is only modestly reduced by tobramycin; hence, the
26 mechanism whereby tobramycin improves lung function is unclear. Here, we demonstrate that
27 tobramycin increases the abundance of two 5' tRNA-fMet halves in outer membrane vesicles
28 (OMVs) secreted by *P. aeruginosa* and that the 5' tRNA-fMet halves reduce IL-8 secretion by
29 CF bronchial epithelial cells (CF-HBECs). In mouse lung, the 5' tRNA-fMet halves attenuate KC
30 secretion and neutrophil recruitment. We also report that the 5' tRNA-fMet halves suppress pro-
31 inflammatory network gene expression by an Argonaut 2 (AGO2)-mediated gene silencing
32 mechanism, thereby reducing IL-8 secretion in CF-HBECs. Moreover, tobramycin reduces the
33 IL-8 concentration and neutrophil content in bronchoalveolar lavage fluid of pwCF. Thus, we
34 conclude that tobramycin improves lung function in part by reducing chronic inflammation and
35 neutrophil-mediated lung damage in pwCF.

36 Introduction

37 *Pseudomonas aeruginosa* is an opportunistic pathogen that infects the lungs of
38 immunocompromised individuals, including those with chronic obstructive pulmonary disease
39 and cystic fibrosis (CF), and is an important cause of acute pneumonia (Williams et al., 2010;
40 Konstan et al., 2012; Lieberman and Lieberman, 2003; Novosad and Barker, 2013; Parker et
41 al., 2016). *P. aeruginosa* is one of the leading causes of nosocomial infections worldwide, and
42 ventilator-associated pneumonia mortality can be as high as 30% in some institutions (Williams
43 et al., 2010). *P. aeruginosa* contributes to 5–10% of the acute exacerbations in COPD, afflicting
44 24 million Americans, and is the 3rd-leading cause of death in the U.S. (Novosad and Barker,
45 2013; Sethi, 2010; Lieberman and Lieberman, 2003). *P. aeruginosa* also chronically colonizes
46 the lungs of ~70-80% of adults with CF, and its presence is strongly associated with reduced
47 forced expiratory volume (FEV₁) and a progressive loss of lung function (Stanton, 2017; Davies
48 and Martin, 2018; Cohen and Prince, 2012)

49 CF is a genetic disease caused by absent or aberrant function of the cystic fibrosis
50 transmembrane conductance regulator (CFTR), which leads to airway periciliary dehydration,
51 increased mucus viscosity, and decreased mucociliary clearance (Stanton, 2017; Stoltz et al.,
52 2015). Insufficient mucociliary clearance causes persistent bacterial infection, non-resolving
53 lung inflammation, and excessive neutrophil recruitment (Hauser et al., 2011; Lin and
54 Kazmierczak, 2017). Chronic neutrophilic airway inflammation damages the lungs by continuous
55 secretion of reactive oxygen species (ROS) and proteases, contributing to bronchiectasis and
56 progressive CF lung function loss (Roesch et al., 2018; Khan et al., 2019). *Pseudomonas*
57 *aeruginosa* is the most common pathogen identified in adult CF lungs (Hauser et al., 2011;
58 Cystic Fibrosis Foundation, 2020), and *P. aeruginosa* respiratory infection correlates with CF
59 lung disease severity and mortality (Emerson et al., 2002; Robinson et al., 2009).

60 Inhaled tobramycin is a commonly used antibiotic to suppress *P. aeruginosa* burden in CF and
61 to ameliorate lung function loss once chronic pulmonary colonization is established (Cystic
62 Fibrosis Foundation, 2020; Davies and Martin, 2018). The long-term use of inhaled tobramycin
63 significantly improves lung function and reduces mortality in people with CF (pwCF) (Sawicki et
64 al., 2012; Bowman, 2002). Inhaled tobramycin is administered in intermittent repeated cycles of
65 28 days on the drug and 28 days off. In a double-blind, placebo-controlled study, lung function
66 improved significantly after the first two weeks of treatment and correlated with a decrease of *P.*
67 *aeruginosa* colony-forming units (CFUs) in sputum by more than 158-fold (Ramsey et al., 1999).
68 Intriguingly, the magnitude of the reduction in bacterial CFUs was less than ten-fold in the third
69 cycle of therapy, although lung function improvement was maintained at a comparable level
70 (Ramsey et al., 1999). Furthermore, an open-label, follow-on trial with adolescent patients and
71 12 treatment cycles revealed that the reduction of *P. aeruginosa* CFUs in sputum only explained
72 11.7% of CF lung function improvement (Moss, 2002). Moreover, a more recent analysis of
73 sputum revealed that tobramycin has no significant effect on *P. aeruginosa* abundance (Nelson
74 et al., 2020). Together, these data suggest that tobramycin improves CF lung function by an
75 unknown mechanism in addition to its bactericidal activity. The goal of this study is to elucidate
76 this mechanism.

77 In the CF lungs, *P. aeruginosa* suppresses the host immune response by secreting outer
78 membrane vesicles (OMVs), which fuse with host cells and deliver virulence factors, DNA, small
79 RNAs (sRNAs), and transfer RNA (tRNA) fragments that mediate inter-kingdom host-pathogen
80 interaction (Li and Stanton, 2021; Kaparakis-Liaskos and Ferrero, 2015; Bomberger et al., 2009;
81 Coelho and Casadevall, 2019). OMVs are 50-300 nm lipopolysaccharide (LPS)-decorated
82 vesicles secreted by all gram-negative bacteria (Coelho and Casadevall, 2019; Jan, 2017).
83 Recently, we reported that *P. aeruginosa* secretes a 24-nucleotides (nt) long sRNA in OMVs,
84 which diffuse through the airway mucus layer and fuse with bronchial epithelial cells to transfer

85 the sRNA (Koeppen et al., 2016). The sRNA down-regulates the OMV-induced secretion of IL-8,
86 a potent neutrophil attractant, by airway epithelial cells, leading to attenuated recruitment of
87 neutrophils into mouse lungs (Koeppen et al., 2016).

88 This study aimed to test the hypothesis that tobramycin prevents the decline in lung function of
89 pwCF by increasing the level of anti-inflammatory sRNAs in OMVs secreted by *P. aeruginosa*.

90 Here, we demonstrate that tobramycin increases the abundance of two 5' formyl-methionine
91 tRNA (tRNA-fMet) halves in OMVs, and that the 5' tRNA-fMet halves are delivered into primary
92 CF-HBECs by OMVs. 5' tRNA-fMet halves suppress IL-8 secretion by CF-HBECs and reduce
93 KC (a murine homolog of IL-8) levels and neutrophil recruitment in mouse lungs by an AGO2-
94 mediated post-transcriptional regulatory mechanism. This 5' tRNA-fMet halves-mediated
95 reduction in lung neutrophils is predicted to mitigate lung damage. In pwCF, the IL-8
96 concentration and neutrophil content in bronchoalveolar lavage fluid (BALF) was significantly
97 reduced during the month of tobramycin administration compared to the month off tobramycin.

98 Taken together, these data reveal that the clinical benefit of tobramycin is due in part to an
99 increase in the secretion of 5' tRNA-fMet halves in OMVs, leading to attenuation of IL-8 and
100 neutrophil-mediated CF lung damage.

101 **Results**

102 **Tobramycin reduces the ability of OMVs secreted by *P. aeruginosa* to stimulate IL-8**
103 **secretion by CF-HBECs.**

104 To test the hypothesis that tobramycin alters the virulence of OMVs secreted by *P. aeruginosa*,
105 we designed an *in vitro* experiment depicted in Figure 1A. *P. aeruginosa* strain PA14 was grown
106 in lysogeny broth (LB), and OMVs secreted by *P. aeruginosa* treated with vehicle (ctrl-OMVs) or
107 tobramycin (Tobi-OMVs) were isolated as described in Methods. The concentration of
108 tobramycin used (1 µg/mL) reduced growth by 33%, an amount similar to that observed in pwCF
109 treated with tobramycin after three cycles of therapy (Ramsey et al., 1999) (Figure 1B).
110 Tobramycin increased the secretion of OMVs by 38% compared to control (Figure 1C), which
111 coincides with a previous report that antibiotics induce OMV production by *P. aeruginosa*
112 (MacDonald and Kuehn, 2013).

113 To examine the effect of OMVs on the host immune response, polarized HBECs from CF
114 donors (CF-HBECs) were grown in air-liquid interface (ALI) culture (Randell et al., 2011;
115 Barnaby et al., 2019) and exposed to the same number of ctrl-OMVs or Tobi-OMVs for 6 hours,
116 whereupon IL-8 secretion was measured. Tobi-OMVs induced 36% less IL-8 secretion than ctrl-
117 OMVs (Figure 1D). Similar results were obtained even when cells were exposed to 40% more
118 Tobi-OMVs (1.4X Tobi-OMVs) than ctrl-OMVs to reflect the finding that tobramycin increased
119 OMV production (Figure 1D). We measured other cytokines secreted by CF-HBECs (EGF,
120 GRO, IL17a, and IP10) in response to ctrl-OMVs and Tobi-OMVs, but of these additional
121 cytokines only IP-10 was significantly reduced by Tobi-OMVs compared to ctrl-OMVs
122 (Supplemental Figure 1).

123 **Tobramycin increases the abundance of 5' tRNA-fMet halves in OMVs, and the tRNA**
124 **halves are transferred from OMVs to CF-HBECs**

125 To test the hypothesis that tobramycin increases the abundance of anti-inflammatory sRNAs in
126 OMVs, we performed a small RNA-sequencing analysis to compare the sRNA content in ctrl-
127 OMVs and Tobi-OMVs. We identified 6145 unique sequences mapped to the PA14 genome,
128 and 1064 were differentially enriched in Tobi-OMVs. The sequence length ranged from 20 to 48
129 nucleotides; however, we excluded the 48-nt sequences from further analysis as they
130 represented RNA species longer than the read length.

131 We focused on the most abundant and differentially induced sRNAs in Tobi-OMVs (Figure 2A
132 and Table 1). We chose two 35-nt long sRNAs (#5 and #7 in Table 1) that were fragments of
133 two initiator tRNAs (tRNA-fMet1 and tRNA-fMet2 located at PA14_62790 and PA14_52320,
134 respectively) in PA14 for further analysis because they were bioinformatically predicted to
135 suppress IL-8 secretion by CF-HBECs. The sequence reads in Tobi-OMVs mapped to these
136 two loci had similar length distributions (Figure 2B and 2C; 80% of reads were 35-nt long),
137 suggesting the tRNA-fMet fragments were not products of random degradation. The similar
138 length distributions also imply common machinery for the biogenesis of these two tRNA
139 fragments. Both have low minimum free energy, suggesting stable secondary structures.

140 The two 35-nt long tRNA-fMet fragments are 5' halves of tRNAs^{fMet} (hereafter called 5' tRNA-
141 fMet halves), which are products of cleavage in the anticodon loop (Figure 2D). Importantly, the
142 two 5' tRNA-fMet halves have high sequence similarity with only one nucleotide difference,
143 suggesting similar sequence-based targeting functions. The high sequence similarity allowed us
144 to design qPCR primers to quantify both 5' tRNA-fMet halves simultaneously. By qPCR, we
145 found that Tobi-OMVs secreted by PA14 and four clinical isolates (including two mucoid strains)
146 also contained significantly more 5' tRNA-fMet halves than ctrl-OMVs (Figure 2E), indicating a
147 strain-independent phenotype that extends to clinically relevant strains. Moreover, we
148 reanalyzed our previously published small RNA-sequencing experiment (Koeppen et al., 2016),
149 in which we sought to detect PA14 sRNAs transferred into non-CF HBECs after ctrl-OMVs

150 exposure, and we were able to identify both 5' tRNA-fMet halves in OMV-exposed cells but not
151 in the un-exposed group (Figure 2F).

152 Taken together, these observations demonstrate that the two 5' tRNA-fMet halves are the most
153 abundant and most differentially induced sRNAs in Tob1-OMVs, have high sequence similarity,
154 and are delivered to airway epithelial cells by OMVs; thus, they are good candidates for further
155 investigation into their possible role in suppressing IL-8 secretion.

156 **5' tRNA-fMet halves reduce IL-8 secretion**

157 To determine if 5' tRNA-fMet halves reduce IL-8 secretion, we transformed PA14 with an
158 arabinose-inducible vector expressing 5' tRNA-fMet1 half (tRNA1-OMVs) or an empty vector
159 control (V-OMVs). Small RNA-sequencing confirmed that the expression of 5' tRNA-fMet1 half
160 in tRNA1-OMVs was significantly induced by 2.73 fold compared to V-OMVs (Supplemental
161 Figure 2). Primary CF-HBECs were exposed to V-OMVs or tRNA1-OMVs, and the secretion of
162 IL-8 was measured by ELISA. As predicted, tRNA1-OMVs induced less IL-8 secretion
163 compared to the same amount of V-OMVs (Figure 3A). To provide additional support for the
164 conclusion that 5' tRNA-fMet halves reduce IL-8 secretion by CF-HBECs, we designed an
165 inhibitor, an RNA oligonucleotide with a complementary sequence to both 5' tRNA-fMet halves.
166 CF-HBECs were transfected with the inhibitor or negative control inhibitor followed by exposure
167 to ctrl-OMVs or 1.4X Tob1-OMVs. As predicted, the inhibitor reduced the ability of 1.4X Tob1-
168 OMVs to suppress IL-8 secretion compared to ctrl-OMVs (Figure 3B).

169 Studies were conducted in mice to further support the conclusion that tobramycin reduces the
170 pro-inflammatory effect of OMVs by increasing the 5' tRNA-fMet1 half content. Mice were
171 exposed to the same number of V-OMVs or tRNA1-OMVs by oropharyngeal aspiration for 5
172 hours, and BALF samples were harvested for analysis. The concentration of KC, a murine
173 functional homolog of IL-8 (Figure 3C), and neutrophil content (Figure 3D) were significantly

174 reduced in BALF obtained from mice exposed to tRNA1-OMVs compared to V-OMVs. Thus, 5'
175 tRNA-fMet1 half reduced the pro-inflammatory response of CF-HBECs *in vitro* and in a mouse
176 model of inflammation.

177 **Inhaled tobramycin has an anti-inflammatory effect in *P. aeruginosa*-infected CF lungs**

178 To determine if tobramycin reduces inflammation and neutrophil burden in CF lungs, we
179 performed a retrospective analysis to assess whether the administration of inhaled tobramycin
180 changes the inflammatory status in pwCF. BALF samples were collected from four CF patients
181 chronically infected with *P. aeruginosa* during the month of inhaled tobramycin (On Tobi) and
182 the month off tobramycin (Off Tobi). In BALF obtained On Tobi, average IL-8 levels were
183 reduced by 48.5% (Figure 3E), and the number of neutrophils was decreased by 25.9% (Figure
184 3F) compared to Off Tobi. This clinical observation is consistent with the *in vitro* and mouse
185 experiments, suggesting that OMVs secreted by tobramycin-exposed *P. aeruginosa* are less
186 pro-inflammatory than control OMVs.

187 **5' tRNA-fMet halves regulate gene expression by base-pairing with target genes in CF- 188 HBECs using an AGO2-mediated mechanism.**

189 Although we and others have shown that prokaryotic sRNAs regulate eukaryotic gene
190 expression in a sequence-specific manner (Koeppen et al., 2016; Maute et al., 2013), the
191 mechanism is unknown. We therefore conducted experiments to determine if *P. aeruginosa* 5'
192 tRNA-fMet halves can utilize the eukaryotic Argonaute 2 (AGO2) dependent gene silencing
193 complex to suppress IL-8 secretion. We designed a three-step approach to identify the RNA
194 binding targets, followed by proteomic analysis to determine the effect of 5' tRNA-fMet halves on
195 protein expression (Figure 4A). Ingenuity Pathway Analysis (IPA) (Krämer et al., 2014) was
196 performed at each step to identify significantly enriched and down-regulated pathways that are
197 relevant to CF and predicted to decrease IL-8 secretion (Table 2).

198 We first performed a miRanda microRNA (miRNA) target scan (Enright et al., 2003) to predict
199 the human binding targets of 5' tRNA-fMet1 half. miRanda is an algorithm designed for RNA-
200 RNA binding prediction considering sequence complementarity and binding free energy. Given
201 the high sequence similarity between the two sRNAs, we used the sequence of 5' tRNA-fMet1
202 half to scan the whole human transcriptome and adjusted the prediction for the gene expression
203 profile of polarized HBE cells to identify a list of 1518 predicted targets, accounting for 8.4% of
204 human coding genes. IPA identified several pro-inflammatory pathways in epithelial cells that
205 are predicted to be down-regulated by 5' tRNA-fMet1 half, including integrin-linked kinase
206 signaling (Eucker et al., 2014; Ahmed et al., 2014; Gravelle et al., 2010), LPS-stimulated MAPK
207 Signaling (Koeppen et al., 2016), and HIF1a signaling (Cane et al., 2010) (Table 2).

208 The target gene prediction and pathway analysis encouraged us to map transcriptome-wide
209 interactions between 5' tRNA-fMet1 half and target mRNAs mediated by AGO2. Although tRNA
210 fragments have been shown to regulate gene expression, to our knowledge, there is no direct
211 evidence that tRNA halves or any small noncoding RNA secreted by a prokaryotic organism can
212 suppress eukaryotic gene expression by interacting with the AGO2 gene silencing complex.
213 Thus, to determine if 5' tRNA-fMet1 half interacts with eukaryotic mRNAs in the AGO2-
214 containing complex, we utilized the enhanced crosslinking and immunoprecipitation (eCLIP)
215 approach (Van Nostrand et al., 2016). Briefly, and as described in detail in methods, this
216 approach involved transfection of 5' tRNA-fMet1 half into CF-HBECs, followed by ligation of 5'
217 tRNA-fMet1 half and other small RNAs to target mRNAs yielding sRNA-mRNA chimeric
218 fragments. Chimeric fragments immunoprecipitated with AGO2 were characterized with high-
219 throughput sequencing (chimeric eCLIP) (Figure 4B), which provided an unprecedented
220 resolution to identify sRNA-mRNA interactions. CF-HBECs were transfected with 5' tRNA-fMet1
221 half or negative control siRNA (siNC) and subjected to AGO2 chimeric eCLIP analysis. This
222 analysis allowed us to profile transcriptome-wide AGO2 authentic binding sites mediated by 5'

223 tRNA-fMet1 half and other miRNAs with a stringent cutoff (IP vs. input cluster log₂ fold
224 enrichment ≥ 3 and P value ≤ 0.001). Using these parameters, we identified 10947 AGO2
225 binding sites in 4454 genes. Within those authentic binding sites, we identified 629 chimeric
226 reads containing at least 18-nt long subsequences of 5' tRNA-fMet1 half. Lengths of identified
227 subsequences ranged from 18-nt to the full size of 5' tRNA-fMet1 half, and alignment positions
228 of subsequences were evenly distributed (Figure 4C). These findings suggest that the full length
229 5' tRNA-fMet1 half was loaded into the AGO2 complex for gene targeting without being pre-
230 processed into a shorter sRNA, and the subsequences with different lengths identified in
231 chimeric reads were products of RNA fragmentation, a key step in the eCLIP sequencing library
232 preparation.

233 To deeply profile the target repertoire of 5' tRNA-fMet1 half mediated by AGO2, we designed a
234 5' tRNA-fMet1 half specific primer, which anneals to most of the identified subsequence (Figure
235 4C), for targeted sequencing (targeted chimeric eCLIP). The targeted chimeric eCLIP allowed
236 us to sequence 5' tRNA-fMet1 half containing chimeric fragment at a much higher depth. We
237 identified that 5' tRNA-fMet1 half targeted 5776 sites in 1945 genes, and those target sites were
238 not found in the negative control (siNC) transfected cells. Interestingly, although miRNA-AGO2
239 complexes usually target 3' untranslated regions (3' UTR), most 5' tRNA-fMet1 half-AGO2 target
240 sites were in introns (Figure 4D). Furthermore, motif enrichment analysis in target sites revealed
241 that nucleotides 16-28 from the 5'-end of 5' tRNA-fMet1 half (which do not include the only
242 distinct nucleotide between the two 5' tRNA-fMet halves) could explain 77% of identified target
243 sites (Figure 4E). The fact that the most popular binding motif does not contain the unique
244 nucleotide differentiating the two 5' tRNA-fMet halves suggests that they have many common
245 target genes. Moreover, we found that miRanda predicted the target genes identified by
246 chimeric eCLIP significantly better than expected by chance (Fisher's exact test, $P < 10^{-12}$),
247 suggesting that bioinformatic target prediction methods based on base-pairing can reliably

248 predict target genes. Also, IPA predicted that a similar set of pro-inflammatory and IL-8
249 induction pathways were inhibited by down-regulating these target genes (Table 2).

250 Lastly, to identify proteins whose abundances were changed by 5' tRNA-fMet halves delivered
251 by OMVs, we utilized OMVs secreted by the 5' tRNA-fMet1 half-overexpression and empty
252 vector clones (Supplemental Figure 2). Primary CF-HBECs from three donors were exposed to
253 V-OMVs or tRNA1-OMVs for 6 hours before being subjected to proteomic analysis. 8343
254 proteins were identified, and we selected the top 20% differentially expressed proteins by *P*
255 value, yielding 943 down-regulated proteins (Figure 4F). The statistically enriched and down-
256 regulated pathways identified by IPA overlapped with our previous analysis based on identified
257 target genes (Table 2). These down-regulated pathways included downstream signaling of
258 IL17A and IL-6, which are pro-inflammatory cytokines secreted by other cell types in CF lungs to
259 induce IL-8 secretion by CF-HBECs (McAllister et al., 2005; Courtney et al., 2004; Hsu et al.).

260 Considering the top 20% down-regulated proteins, IPA identified seven proteins that contributed
261 to IL-8 expression and predicted the decrease of IL-8 secretion (Figure 4G). Among the seven
262 significantly down-regulated proteins, MAPK10, IKBKG, and EP300 were the direct targets of 5'
263 tRNA-fMet1 half identified with our targeted chimeric eCLIP experiment, suggesting targeting of
264 a pro-inflammatory network involving MAPK and NFκB signaling.

265 In summary, our three-step approach demonstrated that 5' tRNA-fMet1 halves transferred from
266 OMVs to CF-HBECs were loaded into the AGO2 complex to target specific genes via a base-
267 pairing mechanism, thus mediating the Tobi-OMVs induced reduction in IL-8 secretion.

268 Discussion

269 The goal of this study was to determine how tobramycin improves clinical outcomes in pwCF
270 without significantly reducing the abundance of *P. aeruginosa*. Our data reveal that tobramycin
271 increases the concentration of 5' tRNA-fMet halves in OMVs secreted by *P. aeruginosa*, that the
272 OMVs deliver 5' tRNA-fMet halves to CF-HBECs, and that the increased delivery of 5' tRNA-
273 fMet halves to CF-HBECs suppresses IL-8 secretion by interacting with pro-inflammatory gene
274 transcripts, including MAPK10, IKBKG, and EP300, in an AGO2-mediated mechanism. Both *in*
275 *vitro* and *in vivo* experiments in mice are consistent with this conclusion. Moreover, our
276 retrospective analysis of pwCF on and off tobramycin is consistent with our data in mice that
277 tobramycin reduces IL-8 and the neutrophil content in BALF. The reduction in the neutrophil
278 content in BALF is predicted to mitigate lung damage in the CF lungs since CF neutrophils are
279 the source of significant lung damage in pwCF (Figure 5). To our knowledge, this is the first
280 report demonstrating that tRNA halves secreted by a prokaryotic organism suppress gene
281 expression in eukaryotic cells by an AGO2-mediated RNA silencing mechanism.

282 tRNA-derived fragments are a novel class of regulatory sRNAs in prokaryotes and eukaryotes
283 (Li and Stanton, 2021; Su et al., 2020). tRNAs are the most abundant RNA species by the
284 number of molecules, and fragments with different lengths have been reported in three domains
285 of life. miRNA-sized (~24-nt long) tRNA fragments in mammalian cells have garnered attention
286 as they have been found to associate with Argonaute (AGO) proteins to mediate gene silencing
287 by base-pairing with target mRNAs (Maute et al., 2013; Kumar et al., 2014; Kuscu et al., 2018).
288 Recently, a report showed that in *Bradyrhizobium japonicum*, a 21-nt tRNA fragment utilizes
289 host plant AGO1 to regulate host gene expression, a cross-kingdom symbiotic relationship
290 between bacteria and plants (Ren et al., 2019). However, tRNA halves have been thought not to
291 involve the AGO-miRNA-like mechanism since they are 32–50 nt in length. tRNA halves have
292 been shown to have both positive and negative effects on translation by regulating the formation

293 of ribosomes and the translation initiation complex (Ivanov et al., 2011; Gebetsberger et al.,
294 2012; Fricker et al., 2019; Mleczko et al., 2018). Here, we provide the first evidence that 35-nt 5'
295 tRNA-fMet halves from a bacterial pathogen are transferred into eukaryotic cells and loaded into
296 AGO2-containing protein complexes without pre-processing into shorter sRNAs to suppress
297 gene expression by base-pairing with target mRNAs. This finding not only provides a novel role
298 of tRNA halves in host-pathogen interactions but also suggests that siRNAs may be an effective
299 therapeutic approach to reduce lung damage caused by chronic inflammation and excessive
300 neutrophil recruitment.

301 The production of tRNA halves, also called tRNA-derived stress-induced RNAs (tiRNAs), by
302 cleavage in the anticodon loop of mature tRNAs is conserved across all life domains in
303 response to various stress conditions (Tao et al., 2020; Fricker et al., 2019; Thompson et al.,
304 2008); however, the molecular mechanism by which prokaryotes sense the stress and cleave
305 specific tRNAs, and the cell-autonomous effects of tRNA halves induced by stress remain
306 largely unknown. *Mycobacterium tuberculosis* maintains its persistence in host cells by cleaving
307 several tRNAs in half with endonucleases VapCs and MazF-mt9 to reduce the level of
308 translation (Winther et al., 2016; Schifano et al., 2016). *Escherichia coli* secretes colicin D, an
309 anticodon ribonuclease (ACNase), to cleave tRNA-Arg of competing *E. coli* strains in half by
310 recognizing the anticodon-loop sequence, and the cleaved tRNA-Arg blocks the ribosome A-site
311 to disrupt translation (Tomita et al., 2000; Ogawa et al., 2020). Similar mechanisms have been
312 identified in fungi to inhibit the cell growth of nonself competitors (Chakravarty et al., 2014; Lu et
313 al., 2005). Together, these reports and our findings suggest that *P. aeruginosa*, in response to
314 tobramycin exposure, up-regulates an unidentified ACNase that recognizes and cleaves the
315 anticodon loop of tRNA-fMets, which are essential initiator tRNAs, to slow down cell growth and
316 prevent cell death.

317 The interaction of *P. aeruginosa* 5' tRNA-fMet halves with CF-HBEC mRNAs by base-pairing is
318 reminiscent of miRNA-mRNA interactions in mammalian cells. While canonical miRNAs use a
319 seed region, typically nucleotides 2-7 of miRNAs, to base-pair with the 3' UTR of target mRNAs
320 (Chipman and Pasquinelli, 2019), we observed that tRNA-fMet halves used nucleotides 16-28 to
321 bind introns and coding sequences of target genes. This finding suggests that more studies are
322 needed to better understand the targeting rule of tRNA halves for more accurate target
323 prediction. Given the high sequence similarity of tRNAs in prokaryotes (Saks and Conery,
324 2007), precise target predictions would help generalize experimental findings to other fragments
325 or pathogens. For example, *Helicobacter pylori* secretes sR-2509025, a 31-nt 5' tRNA-fMet
326 fragment, in OMVs that fuse with human gastric adenocarcinoma cells and sR-2509025
327 diminishes LPS-induced IL-8 secretion (Zhang et al., 2020). Due to the high sequence similarity
328 of tRNA-fMets from *P. aeruginosa* and *H. pylori* and the similar phenotype on regulating IL-8
329 secretion, sR-2509025 may interact with AGO2 in gastric epithelial cells to target the pro-
330 inflammatory network identified in this study.

331 Numerous reports have demonstrated that a myriad of signaling pathways, including NF- κ B and
332 MAPK signaling pathways, induce IL-8 secretion (Lee et al., 2018; Li et al., 2002, 8; Jundi and
333 Greene, 2015). IKBKG, also known as NF- κ B essential modulator (NEMO), is critical for NF- κ B
334 pathway activation. Furthermore, EP300, also called P300, is a transcription co-factor required
335 for NF- κ B-dependent IL-8 induction (Berghe et al., 1999; Huang et al., 2017). Moreover, a study
336 demonstrated that DNA damage leads to NF- κ B activation followed by MAPK10-mediated IL-8
337 secretion (Biton and Ashkenazi, 2011). Indeed, the elevated DNA damage response correlates
338 with the non-resolving neutrophilic inflammation in the CF airways (Brown et al., 1995; Fischer
339 et al., 2013); hence, our findings revealing that 5' tRNA-fMet halves-AGO2 complex decrease
340 IKBKG, EP300, and MAPK10 protein expression and thereby reduce IL-8 secretion and
341 neutrophil levels are consistent with the literature.

342 CFTR is a negative regulator of the pro-inflammatory response mediated by MAPK and NF- κ B
343 signaling. Studies have shown that impaired CFTR leads to overactivation of NF- κ B signaling
344 and enhanced secretion of IL-8 by epithelial cells (DiMango et al., 1998; Vij et al., 2009). Also,
345 CFTR down-regulates thermal injury-induced MAPK/NF- κ B signaling, a pathway that leads to
346 IL-8 expression and pulmonary inflammation (Dong et al., 2015). Here, we demonstrate that 5'
347 tRNA-fMet halves target a pro-inflammatory network involving the MAPK and NF- κ B signaling
348 pathways, which are intrinsically over-activated in CF, highlighting the importance of this
349 network in pulmonary inflammation.

350 There are a few limitations of our study. First, we performed a retrospective analysis of BALF
351 samples collected from pwCF on and off inhaled tobramycin; however, we could not collect
352 BALF in consecutive months on and off tobramycin in the same individuals because of the
353 invasive nature of the technique and IRB restrictions on research bronchoscopies at Dartmouth-
354 Hitchcock Medical Center. Nevertheless, after adjusting the number of days between collection
355 dates for each sample pair (range from 175 to 791 days; Supplemental Table 1), tobramycin-on
356 BALF had significantly lower IL-8 concentration and fewer neutrophil counts than tobramycin-off
357 BALF. Importantly, a similar observation was made for IL-8 in CF sputum samples collected in
358 consecutive months from pwCF on and off tobramycin (Husson et al., 2005). Because studies
359 have shown that IL-8 concentration in sputum is inversely correlated with pulmonary function
360 (Sagel et al., 2002, 2001), we conclude that inhaled tobramycin has an anti-inflammatory effect
361 in *P. aeruginosa*-infected CF lungs, resulting in improved lung function. Second, since there are
362 many other differences in the sRNA content and likely the virulence factor content of Tobi-OMVs
363 compared to ctrl-OMVs, we cannot rule out the possibility that other factors may contribute to
364 the difference in the immune response of CF-HBECs and mouse lungs to Tobi-OMVs versus
365 ctrl-OMVs. Nevertheless, since the inhibitor to 5' tRNA-fMet halves transfected into CF-HBECs
366 blocked the Tobi-OMVs mediated reduction in IL-8 secretion compared to ctrl-OMVs, we

367 conclude that 5' tRNA-fMet halves play a major role in suppressing IL-8 levels and neutrophil
368 recruitment. Third, tRNAs are known to have post-transcriptional modifications, which affect
369 RNA structure and RNA-protein interaction (Lorenz et al., 2017). Whether the modifications on
370 5' tRNA-fMet halves modulate the anti-inflammatory effect requires additional study.

371 Highly effective CFTR modulator drugs have significantly improved outcomes in pwCF;
372 however, in a few recent studies, they have been shown to have either no effect or a modest
373 effect on the *P. aeruginosa* burden in the CF lungs (Davies and Martin, 2018; Yi et al., 2021).
374 Thus, new approaches are needed to reduce the bacterial load in the lungs of chronically
375 colonized pwCF. We propose that 5' tRNA-fMet halves or similar miRNA-like molecules may be
376 utilized as a therapeutic strategy to reduce IL-8 and neutrophil content in the lungs of pwCF,
377 resulting in reduced lung damage and improved lung function.

378 **Methods**

379 ***P. aeruginosa* cultures.** *P. aeruginosa* (strain PA14) and clinical isolates were grown in
380 lysogeny broth (LB, Thermo Fisher Scientific, Waltham, MA) liquid cultures at 37°C with shaking
381 at 225 rpm. Tobramycin (1 µg/mL), a concentration that reduces *P. aeruginosa* by an amount
382 similar to that observed clinically, or vehicle was added to the cultures. The clinical isolates, two
383 mucoid and two non-mucoid strains, have been characterized previously (Yu et al., 2012;
384 Moreau-Marquis et al., 2015). In some experiments, 5' tRNA-fMet1 half (5'-
385 CGCGGGGTGGAGCAGTCTGGTAGCTCGTCGGGCTC-3') was cloned into the arabinose-
386 inducible expression vector pMQ70 (Shanks et al., 2006) by cutting EcoRI and SmaI restriction
387 sites. GenScript (GenScript USA Inc., Piscataway, NJ, USA) performed the cloning procedure.
388 PA14 was transformed with the 5' tRNA-fMet1 half expression vector or empty vector via
389 electroporation. *P. aeruginosa* strains with the arabinose-inducible vector and its derivatives
390 were grown in LB with 133 mM L-arabinose (2% w/v) and 300 µg/ml carbenicillin (both from
391 Sigma-Aldrich).

392 **Growth kinetics of *P. aeruginosa*.** *P. aeruginosa* overnight LB cultures were centrifuged,
393 washed, and resuspended in fresh LB before measuring the optical density at 600 nm (OD600)
394 to determine cell number. Bacteria were seeded at 1×10^5 cells per 100 µl LB with or without
395 tobramycin (1 µg/mL) in a transparent, flat bottom, 96-well plate covered with a lid. The plate
396 was cultured in a plate reader at 37°C for 24 h. The reader was programmed to measure the
397 OD600 every 10 minutes after shaking the plate for 5 seconds.

398 **Outer membrane vesicle preparation and quantification.** OMVs were isolated as described
399 by us previously (Koeppen et al., 2016; Bauman and Kuehn, 2006). Briefly, *P. aeruginosa*
400 overnight cultures were centrifuged for 1 h at 2800 g and 4°C to pellet the bacteria. The
401 supernatant was filtered twice through 0.45 µm PVDF membrane filters (Millipore, Billerica, MA,
402 USA) to remove bacteria and concentrated with 30K Amicon filters (Millipore, Billerica, MA,

403 USA) at 2800 g and 4°C to obtain ~200 µL concentrate. The concentrate was resuspended in
404 OMV buffer (20 mM HEPES, 500 mM NaCl, pH 7.4) and subjected to ultracentrifugation for 2 h
405 at 200,000 g and 4°C to pellet OMVs. OMV pellets were re-suspended in 60% OptiPrep Density
406 Gradient Medium (Sigma-Aldrich, Cat. # D1556) and layered with 40%, 35%, 30% and 20%
407 OptiPrep diluted in OMV buffer. OMVs in OptiPrep layers were centrifuged for 16 h at 100,000 g
408 and 4°C. 500 µl fractions were taken from the top of the gradient, with OMVs residing in
409 fractions 2 and 3, corresponding to 25% OptiPrep. The purified OMVs were quantified by
410 nanoparticle tracking analysis (NTA, NanoSight NS300, Malvern Panalytical Ltd, Malvern, UK)
411 before exposure of CF-HBECs or mice to OMVs.

412 **CF-HBEC culture.** De-identified primary human bronchial epithelial cells from four CF donors
413 (CF-HBECs, Phe508del homozygous) were obtained from Dr. Scott Randell (University of North
414 Carolina, Chapel Hill, NC, USA) and cultured as described previously (Fulcher and Randell,
415 2013; Koeppen et al., 2021). Briefly, cells were grown in BronchiaLife basal medium (Lifeline
416 Cell Technology, Frederick, MD, USA) supplemented with the BronchiaLife B/T LifeFactors Kit
417 (Lifeline) as well as 10,000 U/ml Penicillin and 10,000 µg/ml Streptomycin.

418 To polarize cells, CF-HBECs were seeded on polyester transwell permeable filters (#3405 for
419 24-mm transwell or #3801 for 12-mm Snapwell; Corning, Corning, NY) coated with 50 µg/ml
420 Collagen type IV (Sigma-Aldrich, St. Louis, MO). Air Liquid Interface (ALI) medium was added to
421 both apical and basolateral sides for cell growth. Once a confluent monolayer was obtained, the
422 apical medium was removed, and cells were cultured at an air-liquid interface and fed
423 basolaterally every other day with ALI media for 3-4 weeks before cells were fully polarized for
424 treatment (Randell et al., 2011).

425 **Exposure of cells to OMVs.** Polarized cells on 12-mm Snapwell filters were washed with PBS
426 to remove excess mucus, and 2 mL of serum-free ALI medium was added to the basolateral
427 side. 1.5×10^{10} purified OMVs or the same volume of Optiprep vehicle control in 200 µL serum-

428 free ALI medium were applied to the apical side of cells. 2.1×10^{10} Tobi-OMVs (1.4X Tobi-OMVs)
429 were also used. After a six-hour exposure, the basolateral medium was collected for cytokine
430 measurements.

431 **Cytokine measurements.** Cytokine secretion from primary CF-HBECs was measured with the
432 Human IL-8/CXCL8 DuoSet ELISA (#DY208, R&D Systems, Minneapolis, MN). Several
433 samples were also screened with MILLIPLEX MAP Human Cytokine/Chemokine 41-Plex
434 cytokine assay (Millipore). Cytokines in mouse BALF were analyzed with the Mouse CXCL1/KC
435 DuoSet ELISA (#DY453, R&D Systems, Minneapolis, MN).

436 **RNA isolation and small RNA-seq analysis.** PA14 was grown in T-broth (10 g tryptone and 5
437 g NaCl in 1 L H₂O) with or without tobramycin (1 µg/mL) to reduce small RNA reads from yeast
438 present in LB medium. The culture supernatants were processed as mentioned above to obtain
439 OMV pellets. The pellets were resuspended with OMV buffer and re-pelleted again by
440 centrifugation at 200,000 g for 2 h at 4°C and lysed with Qiazol followed by RNA isolation with
441 the miRNeasy kit (Qiagen) to obtain total RNA including the small RNA fraction. DNase-treated
442 total RNA was used to prepare cDNA libraries with the SMARTer smRNA-Seq Kit (Takara Bio,
443 Mountain View, CA). Libraries were sequenced as 50 bp single-end reads on an Illumina HiSeq
444 sequencer. The first three nucleotides of all reads and the adapter sequences were trimmed
445 using cutadapt (Martin, 2011) before sequence alignment.

446 To verify the overexpression of 5' tRNA-fMet1 half, PA14 clones with the 5' tRNA-fMet1 half
447 expression plasmid or the empty pMQ70 vector were grown in LB (with L-arabinose and
448 carbenicillin) for isolation of V-OMVs and tRNA1-OMVs. The OMV pellets were collected and
449 processed as described above to isolate RNA. The QIAseq miRNA Library Kit (Qiagen) was
450 used to prepare cDNA libraries, and 50 bp single-end sequencing was performed on an Illumina
451 MiniSeq system.

452 Reads were aligned to the PA14 reference genome using CLC Genomics Workbench (CLC-
453 Bio/Qiagen) with the following modifications from the standard parameters: a) the maximum
454 number of mismatches = zero to eliminate unspecific alignment and b) the maximum number of
455 hits for a read = 30 to capture all sRNAs aligned to the PA14 genome. Pileups of mapped reads
456 and frequency tables for each unique sequence were exported for normalization and further
457 analysis with the software package edgeR in the R environment (R Core Team, 2021; Robinson
458 et al., 2010).

459 **Detection of 5' tRNA-fMet halves by RT-PCR.** The induction of 5' tRNA-fMet halves by
460 tobramycin in OMVs of different *P. aeruginosa* strains was detected by custom Taqman Small
461 RNA Assay (#4398987, Thermo Fisher Scientific). According to the manufacturer's instructions,
462 cDNA was synthesized with the TaqMan MicroRNA Reverse Transcription Kit (#4366596,
463 Thermo Fisher Scientific). PCR amplification and detection of 5' tRNA-fMet halves were
464 performed using the TaqMan Universal PCR Master Mix (#4304437, Thermo Fisher Scientific)
465 as well as custom primers and probe design to target both 5' tRNA-fMet halves specifically.

466 **5' tRNA-fMet1 half target prediction.** The miRanda microRNA target scanning algorithm
467 (v3.3a) was used to predict human target genes of 5' tRNA-fMet1 half (Enright et al., 2003). The
468 5' tRNA-fMet1 half sequence was scanned against human RNA sequences (annotations from
469 GRCh38.p13 assembly) with a minimum miRanda alignment score of 150 to generate a list of
470 predicted target genes and the corresponding interaction minimum free energies. To account for
471 the effect of gene expression on target prediction, for each predicted target the minimum free
472 energy was multiplied by the gene expression level (log2CPM) in polarized HBECs identified in
473 our previous publication (Goodale et al., 2017) to obtain an energy-expression score. 1518
474 genes (8.4% of all human genes) with energy-expression scores small than -200 were defined
475 as predicted targets for the Ingenuity Pathway Analysis (Krämer et al., 2014).

476 **Transfection of CF-HBECs with 5' tRNA-fMet1 half and chimeric eCLIP analysis**

477 CF-HBECs were seeded on 15 cm dishes coated with PureCol Bovine Collagen Solution
478 (Advanced BioMatrix, Carlsbad, CA, USA) at 2.7×10^6 cells per dish. Three days after seeding
479 (at 80% confluence), cells were washed and fed with complete Lifeline medium with antibiotics
480 and transfected with 100 nM 5' tRNA-fMet1 half (#10620310, Invitrogen custom siRNA, Thermo
481 Fisher Scientific) or 100 nM AllStars Negative Control siRNA (siNC) using HiPerFect
482 transfection reagent (both from Qiagen). One day after transfection, cells were washed and
483 covered with room temperature PBS before UV irradiation (254 nm, 400 mJ/cm²). The irradiated
484 cells were partially digested with pre-warmed 37°C trypsin/EDTA followed by addition of cold
485 soybean trypsin inhibitor solution to round up cells before collection with scrapers and
486 centrifugation at 600 x g for 10 minutes at 4°C. Cell pellets were flash-frozen in liquid nitrogen
487 and shipped to Eclipse BioInnovations for chimeric eCLIP (Eclipse BioInnovations, San Diego,
488 CA).

489 The chimeric eCLIP experiment and initial data analysis were conducted by Eclipse
490 BioInnovations (Eclipse BioInnovations, San Diego, CA) as previously described (Van Nostrand
491 et al., 2016) with an additional ligation step to form chimeric RNA-RNA species before 3' RNA
492 adapter ligation. In brief, cells were lysed and digested with RNase I. For each cell pellet, an
493 input and an immunoprecipitated sample using an anti-AGO2 antibody (Eclipse BioInnovations,
494 San Diego, CA) were generated for cDNA library preparation followed by paired-end 150 bp
495 sequencing on a NovaSeq platform. Non-chimeric reads were mapped to the human genome
496 (UCSC version GRCh38/hg38), AGO2 binding clusters were identified by CLIPper (Lovci et al.,
497 2013) in immunoprecipitated (IP) samples and normalized against the paired input sample to
498 define significant peaks (\log_2 fold change ≥ 3 of normalized reads and P value < 0.001
499 determined by Fisher's exact test). 5' tRNA-fMet1 half-containing chimeric reads with at least 18
500 nt subsequences of 5' tRNA-fMet1 half were identified, and the subsequences were trimmed
501 before mapping to the human genome.

502 For targeted chimeric eCLIP, a target-specific primer 5' GGGTGGAGCAGTCTGGTA and a
503 sequencing adapter-specific primer were used to enrich 5' tRNA-fMet1 half-containing cDNA
504 from the IP sample libraries before paired-end 150 bp sequencing on a NovaSeq platform. The
505 primer sequence was trimmed from the 5' ends of reads, and the remainder of reads were
506 analyzed as non-chimeric reads as described above. The significant peak regions were
507 identified using the same cutoffs, and HOMER's findMotifsGenome.pl program was used for
508 motif enrichment analysis (Heinz et al., 2010). The resulting list of target genes with significant
509 peaks in the transcripts was used as input for Ingenuity Pathway Analysis.

510 **Proteomic analysis.** Primary CF-HBECs were polarized on 24 mm transwell filters and washed
511 with PBS before treatment. 2 mL serum-free ALI medium was added to the basolateral side.
512 2.8×10^{10} purified V-OMVs or tRNA1-OMVs in 800 μ L serum-free ALI medium were applied to
513 the apical side of cells. After a six-hour exposure, the cells were washed with PBS and
514 detached from the transwells with pre-warmed 37°C trypsin/EDTA. Cells were pelleted and
515 flash-frozen in liquid nitrogen for proteomic analysis.

516 The cell pellets were lysed in 8M urea/50mM Tris pH 8.1/100mM NaCl + protease inhibitors
517 (Roche) and quantified by BCA assay (Pierce), followed by trypsin digestion and desalting. 40
518 micrograms of peptides from each pellet were labeled with unique TMT reagent isobars; the
519 individual TMT-labeled samples were then combined and fractionated offline into 12 fractions by
520 PFP-RP-LC (Grassetti et al., 2017), followed by analysis on a UPLC-Orbitrap Fusion Lumos
521 tribrid instrument in SPS-MS3 mode (McAlister et al., 2014). The resulting tandem mass spectra
522 were data-searched using Comet; TMT reporter ion intensities were summed for each protein
523 and normalized for total intensity across all channels. Mean fold changes comparing tRNA1-
524 OMV-exposed cells with V-OMVs-exposed cells were calculated for each protein detected in all
525 samples. Proteins were ranked by paired t-test *P* value, and network analysis of the top 20%
526 proteins was performed with Ingenuity Pathway Analysis.

527 **Transfection of CF-HBECs with 5' tRNA-fMet halves inhibitor and OMV exposure.** CF-
528 HBECs were seeded on PureCol-coated 12-well plates (Corning Inc.) at 50,000 cells per well.
529 Two days after seeding (~80% confluence), cells were washed and fed with the complete
530 Lifeline medium plus antibiotics and transfected with 50 nM custom mirVana miRNA inhibitor
531 (inhibitor sequence: 5'- GAGCCCGACGAGCUACCAGACUGCUCCA-3', #4464086, Thermo
532 Fisher Scientific) or 50 nM mirVanna inhibitor negative control#1 (#4464077, Thermo Fisher
533 Scientific) using HiPerFect transfection reagent (Qiagen). 6 hours after transfection, cells were
534 exposed to Optiprep vehicle ctrl, ctrl-OMVs (0.4×10^{10} per well), 1.4X Tobi-OMVs (0.55×10^{10} per
535 well) for another 6 h, and the supernatants were collected for cytokine measurements.

536 **Mouse exposure to OMVs**

537 All animal experiments were approved by the Dartmouth Institutional Animal Care and Use
538 Committee (Protocol No. 00002026). 8–9 weeks old male and female C57BL/6J mice (The
539 Jackson Laboratory, Bar Harbor, ME, USA) were inoculated by oropharyngeal aspiration with
540 OMVs (0.5×10^{10} OMVs per mouse) or vehicle following brief anesthesia with isoflurane. OMV
541 concentrations were adjusted with PBS to obtain 50 μ l inoculation volume. 5 h after exposure,
542 mice were euthanized using isoflurane anesthesia, followed by cervical dislocation after
543 breathing stops. Mice trachea were surgically exposed, and a catheter tube was inserted into
544 the trachea and stabilized with sutures (#100–5000, Henry Schein Inc., Melville, NY, USA). The
545 catheter was prepared by fitting a 23 gauge needle (BD #305145, Becton, Dickinson and
546 Company, Franklin Lakes, NJ, USA) into transparent plastic tubing (BD #427411). BALF was
547 collected by pumping 1 ml of sterile PBS into the lungs and recovered with a syringe (BD
548 #309659). This process was repeated once to collect 2 mL of BALF.

549 **Human subjects and bronchoscopy.** All CF subjects were enrolled in a protocol approved by
550 the Dartmouth Hitchcock Institutional Review Board (Protocol No. 22781). CF subjects
551 (Phe508del homozygous) prescribed with an inhaled tobramycin regimen were enrolled if they

552 had an FEV1 > 50% predicted, and were not currently having an exacerbation. Following
553 informed consent, local anesthesia with nebulized lidocaine was administered to the posterior
554 pharynx. Under conscious sedation, a flexible fiberoptic bronchoscopy was performed
555 transorally. BALF was obtained from tertiary airways. After the bronchoscopy procedure, CF
556 subjects were monitored per institutional protocol until they were stable for discharge.

557 **Quantification of neutrophils in BALF.** Cells in BALF samples were pelleted and
558 resuspended in 100 μ L RBC lysis buffer (Promega) for 1 min. After removing red blood cells, the
559 total number of cells in each BALF sample was counted, and concentrations were adjusted.
560 2×10^5 cells per sample were spun onto glass slides, air-dried, and stained with the Differential
561 Quik Stain Kit (Polysciences, Warrington, PA) according to the manufacturer's protocol.
562 Neutrophils were counted under 100x magnification using a microscope. The neutrophil
563 concentration of BALF was calculated by accounting for the retrieved BALF volume and the
564 dilution factors used to adjust the cell concentration.

565 **Statistics.** Data were analyzed using the R software environment for statistical computing and
566 graphics version 4.1.0 (R Core Team, 2021) and Ingenuity Pathway Analysis (Krämer et al.,
567 2014). Statistical significance was calculated using a mixed effect linear model, Wilcoxon rank-
568 sum tests, paired t-tests, and likelihood ratio tests on gene-wise negative binomial generalized
569 linear models, as indicated in the figure legends. Data were visualized, and figures were created
570 using the R package ggplot2 (Wickham, 2016, 2).

571 **Supplemental material.** Fig. S1 contains data on the effect of Tobi-OMVs on cytokines
572 secreted by CF-HBEC. Fig. S2 provides validation that the 5' tRNA-fMet1 half are over-
573 expressed in OMVs. Table S1 contains the human BALF sample collection dates.

574 **Data availability.** Small RNA-seq and chimera eCLIP data are available from the Gene
575 Expression Omnibus database (accession number GSE183895, GSE183897, and
576 GSE183898).

577

578

579

580

581 **Author contributions**

582 ZL, KK, AA, DAH, SAG, and BAS designed the research studies. ZL and KK conducted
583 experiments, acquired data, and analyzed data. AA recruited human subjects, collected clinical
584 samples and data for analysis. SAG performed the proteomic experiment. ZL prepared figures.
585 ZL, KK, AA, DAH, SAG, and BAS wrote the manuscript. All authors contributed to the article and
586 approved the submitted version.

587 **Acknowledgments**

588 This work was supported by the Cystic Fibrosis Foundation (STANTO19G0, STANTO20PO,
589 STANTO19R0, and HOGAN19G0), the NIH (P30-DK117469, R01HL151385, P20-GM113132,
590 S10OD016262), and NCCC Cancer Center Core Grants (5P30 CA023108-41, P30CA023108).
591 We thank Dr. Fred W. Kolling for advice and support on the RNA-seq experiments.

592 **Reference**

- 593 Ahmed, A.U., S.T. Sarvestani, M.P. Gantier, B.R.G. Williams, and G.E. Hannigan. 2014.
594 Integrin-linked Kinase Modulates Lipopolysaccharide- and *Helicobacter pylori*-
595 induced Nuclear Factor κ B-activated Tumor Necrosis Factor- α Production via
596 Regulation of p65 Serine 536 Phosphorylation. *Journal of Biological Chemistry*.
597 289:27776–27793. doi:10.1074/jbc.M114.574541.
- 598 Barnaby, R., K. Koeppen, and B.A. Stanton. 2019. Cyclodextrins reduce the ability of
599 *Pseudomonas aeruginosa* outer-membrane vesicles to reduce CFTR Cl-
600 secretion. *American Journal of Physiology-Lung Cellular and Molecular*
601 *Physiology*. 316:L206–L215. doi:10.1152/ajplung.00316.2018.
- 602 Bauman, S.J., and M.J. Kuehn. 2006. Purification of outer membrane vesicles from
603 *Pseudomonas aeruginosa* and their activation of an IL-8 response. *Microbes and*
604 *Infection*. 8:2400–2408. doi:10.1016/j.micinf.2006.05.001.
- 605 Berghe, W.V., K.D. Bosscher, E. Boone, S. Plaisance, and G. Haegeman. 1999. The
606 Nuclear Factor- κ B Engages CBP/p300 and Histone Acetyltransferase Activity for
607 Transcriptional Activation of the Interleukin-6 Gene Promoter. *Journal of*
608 *Biological Chemistry*. 274:32091–32098. doi:10.1074/jbc.274.45.32091.
- 609 Biton, S., and A. Ashkenazi. 2011. NEMO and RIP1 Control Cell Fate in Response to
610 Extensive DNA Damage via TNF- α Feedforward Signaling. *Cell*. 145:92–103.
611 doi:10.1016/j.cell.2011.02.023.
- 612 Bomberger, J.M., D.P. MacEachran, B.A. Coutermarsh, S. Ye, G.A. O’Toole, and B.A.
613 Stanton. 2009. Long-Distance Delivery of Bacterial Virulence Factors by
614 *Pseudomonas aeruginosa* Outer Membrane Vesicles. *PLOS Pathogens*.
615 5:e1000382. doi:10.1371/journal.ppat.1000382.
- 616 Bowman, C.M. 2002. The long-term use of inhaled tobramycin in patients with cystic
617 fibrosis. *Journal of Cystic Fibrosis*. 1:194–198. doi:10.1016/S1569-
618 1993(02)00003-6.
- 619 Brown, R.K., A. McBurney, J. Lunec, and F.J. Kelly. 1995. Oxidative damage to DNA in
620 patients with cystic fibrosis. *Free Radical Biology and Medicine*. 18:801–806.
621 doi:10.1016/0891-5849(94)00172-G.
- 622 Cane, G., A. Ginouvès, S. Marchetti, R. Buscà, J. Pouysségur, E. Berra, P. Hofman,
623 and V. Vouret-Craviari. 2010. HIF-1 α mediates the induction of IL-8 and VEGF
624 expression on infection with Afa/Dr diffusely adhering *E. coli* and promotes EMT-
625 like behaviour. *Cellular Microbiology*. 12:640–653. doi:10.1111/j.1462-
626 5822.2009.01422.x.
- 627 Chakravarty, A.K., P. Smith, R. Jalan, and S. Shuman. 2014. Structure, Mechanism,
628 and Specificity of a Eukaryal tRNA Restriction Enzyme Involved in Self-Nonself
629 Discrimination. *Cell Reports*. 7:339–347. doi:10.1016/j.celrep.2014.03.034.

- 630 Chipman, L.B., and A.E. Pasquinelli. 2019. miRNA Targeting: Growing beyond the
631 Seed. *Trends in Genetics*. 35:215–222. doi:10.1016/j.tig.2018.12.005.
- 632 Coelho, C., and A. Casadevall. 2019. Answers to naysayers regarding microbial
633 extracellular vesicles. *Biochemical Society Transactions*. 47:1005–1012.
634 doi:10.1042/BST20180252.
- 635 Cohen, T.S., and A. Prince. 2012. Cystic fibrosis: a mucosal immunodeficiency
636 syndrome. *Nat Med*. 18:509–519. doi:10.1038/nm.2715.
- 637 Courtney, J.M., M. Ennis, and J.S. Elborn. 2004. Cytokines and inflammatory mediators
638 in cystic fibrosis. *Journal of Cystic Fibrosis*. 3:223–231.
639 doi:10.1016/j.jcf.2004.06.006.
- 640 Cystic Fibrosis Foundation. 2020. Cystic Fibrosis Foundation Patient Registry 2019
641 Annual Data Report. *Cystic Fibrosis Foundation, Bethesda, MD*. 92.
- 642 Davies, J.C., and I. Martin. 2018. New anti-pseudomonal agents for cystic fibrosis- still
643 needed in the era of small molecule CFTR modulators? *Expert Opinion on*
644 *Pharmacotherapy*. 19:1327–1336. doi:10.1080/14656566.2018.1505864.
- 645 DiMango, E., A.J. Ratner, R. Bryan, S. Tabibi, and A. Prince. 1998. Activation of NF-
646 kappaB by adherent *Pseudomonas aeruginosa* in normal and cystic fibrosis
647 respiratory epithelial cells. *J. Clin. Invest*. 101:2598–2605. doi:10.1172/JCI2865.
- 648 Dong, Z.W., J. Chen, Y.C. Ruan, T. Zhou, Y. Chen, Y. Chen, L.L. Tsang, H.C. Chan,
649 and Y.Z. Peng. 2015. CFTR-regulated MAPK/NF-κB signaling in pulmonary
650 inflammation in thermal inhalation injury. *Sci Rep*. 5. doi:10.1038/srep15946.
- 651 Emerson, J., M. Rosenfeld, S. McNamara, B. Ramsey, and R.L. Gibson. 2002.
652 *Pseudomonas aeruginosa* and other predictors of mortality and morbidity in
653 young children with cystic fibrosis. *Pediatric Pulmonology*. 34:91–100.
654 doi:10.1002/ppul.10127.
- 655 Enright, A.J., B. John, U. Gaul, T. Tuschl, C. Sander, and D.S. Marks. 2003. MicroRNA
656 targets in *Drosophila*. *Genome Biology*. 5:R1. doi:10.1186/gb-2003-5-1-r1.
- 657 Eucker, T.P., D.R. Samuelson, M. Hunzicker-Dunn, and M.E. Konkel. 2014. The focal
658 complex of epithelial cells provides a signalling platform for interleukin-8
659 induction in response to bacterial pathogens. *Cellular Microbiology*. 16:1441–
660 1455. doi:https://doi.org/10.1111/cmi.12305.
- 661 Fischer, B.M., J.K. Wong, S. Degan, A.B. Kummarapurugu, S. Zheng, P. Haridass, and
662 J.A. Voynow. 2013. Increased expression of senescence markers in cystic
663 fibrosis airways. *American Journal of Physiology-Lung Cellular and Molecular*
664 *Physiology*. 304:L394–L400. doi:10.1152/ajplung.00091.2012.

- 665 Fricker, R., R. Brogli, H. Luidalepp, L. Wyss, M. Fasnacht, O. Joss, M. Zywicki, M.
666 Helm, A. Schneider, M. Cristodero, and N. Polacek. 2019. A tRNA half modulates
667 translation as stress response in *Trypanosoma brucei*. *Nature Communications*.
668 10:118. doi:10.1038/s41467-018-07949-6.
- 669 Fulcher, M.L., and S.H. Randell. 2013. Human Nasal and Tracheo-Bronchial
670 Respiratory Epithelial Cell Culture. *In* *Epithelial Cell Culture Protocols: Second*
671 *Edition*. S.H. Randell and M.L. Fulcher, editors. Humana Press, Totowa, NJ.
672 109–121.
- 673 Gebetsberger, J., M. Zywicki, A. Künzi, and N. Polacek. 2012. tRNA-Derived Fragments
674 Target the Ribosome and Function as Regulatory Non-Coding RNA in *Haloferax*
675 *volcanii*. *Archaea*. 2012:e260909. doi:<https://doi.org/10.1155/2012/260909>.
- 676 Goodale, B.C., E.J. Rayack, and B.A. Stanton. 2017. Arsenic alters transcriptional
677 responses to *Pseudomonas aeruginosa* infection and decreases antimicrobial
678 defense of human airway epithelial cells. *Toxicol Appl Pharmacol*. 331:154–163.
679 doi:10.1016/j.taap.2017.06.010.
- 680 Grassetti, A.V., R. Hards, and S.A. Gerber. 2017. Offline pentafluorophenyl (PFP)-RP
681 prefractionation as an alternative to high-pH RP for comprehensive LC-MS/MS
682 proteomics and phosphoproteomics. *Anal Bioanal Chem*. 409:4615–4625.
683 doi:10.1007/s00216-017-0407-6.
- 684 Gravelle, S., R. Barnes, N. Hawdon, L. Shewchuk, J. Eibl, J.S. Lam, and M. Ulanova.
685 2010. Up-regulation of integrin expression in lung adenocarcinoma cells caused
686 by bacterial infection: in vitro study. *Innate Immun*. 16:14–26.
687 doi:10.1177/1753425909106170.
- 688 Gruber, A.R., R. Lorenz, S.H. Bernhart, R. Neuböck, and I.L. Hofacker. 2008. The
689 Vienna RNA Websuite. *Nucleic Acids Research*. 36:W70–W74.
690 doi:10.1093/nar/gkn188.
- 691 Hauser, A.R., M. Jain, M. Bar-Meir, and S.A. McColley. 2011. Clinical Significance of
692 Microbial Infection and Adaptation in Cystic Fibrosis. *Clin Microbiol Rev*. 24:29–
693 70. doi:10.1128/CMR.00036-10.
- 694 Heinz, S., C. Benner, N. Spann, E. Bertolino, Y.C. Lin, P. Laslo, J.X. Cheng, C. Murre,
695 H. Singh, and C.K. Glass. 2010. Simple combinations of lineage-determining
696 transcription factors prime cis-regulatory elements required for macrophage and
697 B cell identities. *Mol Cell*. 38:576–589. doi:10.1016/j.molcel.2010.05.004.
- 698 Hsu, D., P. Taylor, D. Fletcher, R. van Heeckeren, J. Eastman, A. van Heeckeren, P.
699 Davis, J.F. Chmiel, E. Pearlman, and T.L. Bonfield. Interleukin-17
700 Pathophysiology and Therapeutic Intervention in Cystic Fibrosis Lung Infection
701 and Inflammation. *Infection and Immunity*. 84:2410–2421. doi:10.1128/IAI.00284-
702 16.

- 703 Huang, Z.-W., G.-S. Lien, C.-H. Lin, C.-P. Jiang, and B.-C. Chen. 2017. p300 and
704 C/EBP β -regulated IKK β expression are involved in thrombin-induced IL-8/CXCL8
705 expression in human lung epithelial cells. *Pharmacological Research*. 121:33–41.
706 doi:10.1016/j.phrs.2017.04.020.
- 707 Husson, M.O., N. Wizla-Derambure, D. Turck, P. Gosset, and B. Wallaert. 2005. Effect
708 of intermittent inhaled tobramycin on sputum cytokine profiles in cystic fibrosis.
709 *Journal of Antimicrobial Chemotherapy*. 56:247–249. doi:10.1093/jac/dki179.
- 710 Ivanov, P., M.M. Emara, J. Villen, S.P. Gygi, and P. Anderson. 2011. Angiogenin-
711 Induced tRNA Fragments Inhibit Translation Initiation. *Molecular Cell*. 43:613–
712 623. doi:10.1016/j.molcel.2011.06.022.
- 713 Jan, A.T. 2017. Outer Membrane Vesicles (OMVs) of Gram-negative Bacteria: A
714 Perspective Update. *Front. Microbiol*. 8. doi:10.3389/fmicb.2017.01053.
- 715 Jundi, K., and C.M. Greene. 2015. Transcription of Interleukin-8: How Altered
716 Regulation Can Affect Cystic Fibrosis Lung Disease. *Biomolecules*. 5:1386–
717 1398. doi:10.3390/biom5031386.
- 718 Kaparakis-Liaskos, M., and R.L. Ferrero. 2015. Immune modulation by bacterial outer
719 membrane vesicles. *Nature Reviews Immunology*. 15:375–387.
720 doi:10.1038/nri3837.
- 721 Khan, M.A., Z.S. Ali, N. Swezey, H. Grasemann, and N. Palaniyar. 2019. Progression
722 of Cystic Fibrosis Lung Disease from Childhood to Adulthood: Neutrophils,
723 Neutrophil Extracellular Trap (NET) Formation, and NET Degradation. *Genes*.
724 10:183. doi:10.3390/genes10030183.
- 725 Koeppen, K., T.H. Hampton, M. Jarek, M. Scharfe, S.A. Gerber, D.W. Mielcarz, E.G.
726 Demers, E.L. Dolben, J.H. Hammond, D.A. Hogan, and B.A. Stanton. 2016. A
727 Novel Mechanism of Host-Pathogen Interaction through sRNA in Bacterial Outer
728 Membrane Vesicles. *PLOS Pathogens*. 12:e1005672.
729 doi:10.1371/journal.ppat.1005672.
- 730 Koeppen, K., A. Nymon, R. Barnaby, Z. Li, T.H. Hampton, A. Ashare, and B.A. Stanton.
731 2021. CF monocyte-derived macrophages have an attenuated response to
732 extracellular vesicles secreted by airway epithelial cells. *American Journal of
733 Physiology-Lung Cellular and Molecular Physiology*. 320:L530–L544.
734 doi:10.1152/ajplung.00621.2020.
- 735 Konstan, M.W., J.S. Wagener, D.R. VanDevanter, D.J. Pasta, A. Yegin, L. Rasouliyan,
736 and W.J. Morgan. 2012. Risk factors for rate of decline in FEV1 in adults with
737 cystic fibrosis. *Journal of Cystic Fibrosis*. 11:405–411.
738 doi:10.1016/j.jcf.2012.03.009.

- 739 Krämer, A., J. Green, J. Pollard, and S. Tugendreich. 2014. Causal analysis
740 approaches in Ingenuity Pathway Analysis. *Bioinformatics*. 30:523–530.
741 doi:10.1093/bioinformatics/btt703.
- 742 Kumar, P., J. Anaya, S.B. Mudunuri, and A. Dutta. 2014. Meta-analysis of tRNA derived
743 RNA fragments reveals that they are evolutionarily conserved and associate with
744 AGO proteins to recognize specific RNA targets. *BMC Biology*. 12:78.
745 doi:10.1186/s12915-014-0078-0.
- 746 Kuscu, C., P. Kumar, M. Kiran, Z. Su, A. Malik, and A. Dutta. 2018. tRNA fragments
747 (tRFs) guide Ago to regulate gene expression post-transcriptionally in a Dicer-
748 independent manner. *RNA*. 24:1093–1105. doi:10.1261/rna.066126.118.
- 749 Lee, J., Y.J. Yoon, J.H. Kim, N.T.H. Dinh, G. Go, S. Tae, K.-S. Park, H.T. Park, C. Lee,
750 T.-Y. Roh, D. Di Vizio, and Y.S. Gho. 2018. Outer Membrane Vesicles Derived
751 From *Escherichia coli* Regulate Neutrophil Migration by Induction of Endothelial
752 IL-8. *Front Microbiol*. 9:2268. doi:10.3389/fmicb.2018.02268.
- 753 Li, J., S. Kartha, S. Iasvovskaia, A. Tan, R.K. Bhat, J.M. Manaligod, K. Page, A.R.
754 Brasier, and M.B. Hershenson. 2002. Regulation of human airway epithelial cell
755 IL-8 expression by MAP kinases. *American Journal of Physiology-Lung Cellular
756 and Molecular Physiology*. 283:L690–L699. doi:10.1152/ajplung.00060.2002.
- 757 Li, Z., and B.A. Stanton. 2021. Transfer RNA-Derived Fragments, the Underappreciated
758 Regulatory Small RNAs in Microbial Pathogenesis. *Front. Microbiol*. 12.
759 doi:10.3389/fmicb.2021.687632.
- 760 Lieberman, D., and D. Lieberman. 2003. Pseudomonal Infections in Patients with
761 COPD. *Treat Respir Med*. 2:459–468. doi:10.1007/BF03256673.
- 762 Lin, C.K., and B.I. Kazmierczak. 2017. Inflammation: A Double-Edged Sword in the
763 Response to *Pseudomonas aeruginosa* Infection. *JIN*. 9:250–261.
764 doi:10.1159/000455857.
- 765 Lorenz, C., C.E. Lünse, and M. Mörl. 2017. tRNA Modifications: Impact on Structure
766 and Thermal Adaptation. *Biomolecules*. 7:35. doi:10.3390/biom7020035.
- 767 Lovci, M.T., D. Ghanem, H. Marr, J. Arnold, S. Gee, M. Parra, T.Y. Liang, T.J. Stark,
768 L.T. Gehman, S. Hoon, K.B. Massirer, G.A. Pratt, D.L. Black, J.W. Gray, J.G.
769 Conboy, and G.W. Yeo. 2013. Rbfox proteins regulate alternative mRNA splicing
770 through evolutionarily conserved RNA bridges. *Nat Struct Mol Biol*. 20:1434–
771 1442. doi:10.1038/nsmb.2699.
- 772 Lu, J., B. Huang, A. Esberg, M.J.O. Johansson, and A.S. Byström. 2005. The
773 *Kluyveromyces lactis* γ -toxin targets tRNA anticodons. *RNA*. 11:1648–1654.
774 doi:10.1261/rna.2172105.

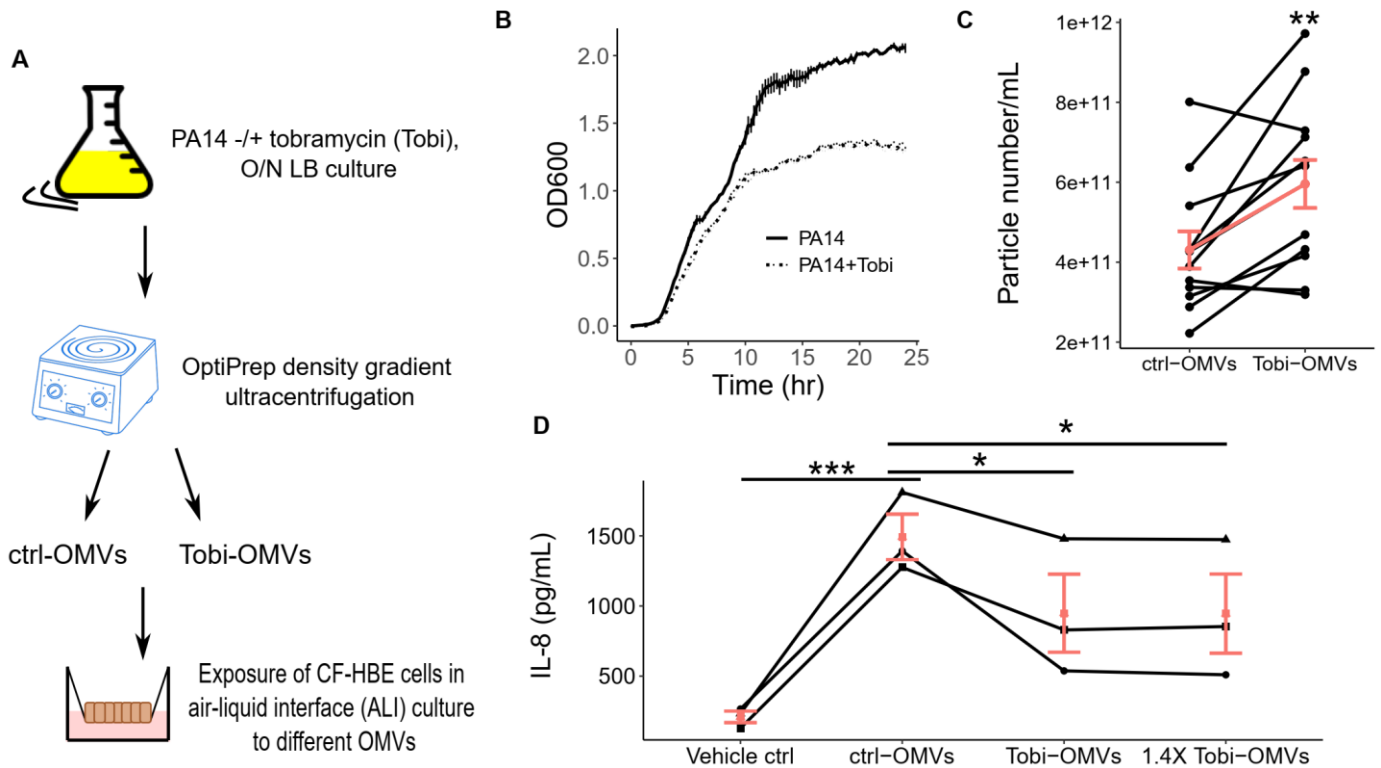
- 775 MacDonald, I.A., and M.J. Kuehn. 2013. Stress-Induced Outer Membrane Vesicle
776 Production by *Pseudomonas aeruginosa*. *Journal of Bacteriology*. 195:2971–
777 2981. doi:10.1128/JB.02267-12.
- 778 Martin, M. 2011. Cutadapt removes adapter sequences from high-throughput
779 sequencing reads. *EMBnet.journal*. 17:10–12. doi:10.14806/ej.17.1.200.
- 780 Maute, R.L., C. Schneider, P. Sumazin, A. Holmes, A. Califano, K. Basso, and R. Dalla-
781 Favera. 2013. tRNA-derived microRNA modulates proliferation and the DNA
782 damage response and is down-regulated in B cell lymphoma. *PNAS*. 110:1404–
783 1409. doi:10.1073/pnas.1206761110.
- 784 McAlister, G.C., D.P. Nusinow, M.P. Jedrychowski, M. Wühr, E.L. Huttlin, B.K. Erickson,
785 R. Rad, W. Haas, and S.P. Gygi. 2014. MultiNotch MS3 Enables Accurate,
786 Sensitive, and Multiplexed Detection of Differential Expression across Cancer
787 Cell Line Proteomes. *Anal. Chem*. 86:7150–7158. doi:10.1021/ac502040v.
- 788 McAllister, F., A. Henry, J.L. Kreindler, P.J. Dubin, L. Ulrich, C. Steele, J.D. Finder, J.M.
789 Pilewski, B.M. Carreno, S.J. Goldman, J. Pirhonen, and J.K. Kolls. 2005. Role of
790 IL-17A, IL-17F, and the IL-17 Receptor in Regulating Growth-Related Oncogene-
791 α and Granulocyte Colony-Stimulating Factor in Bronchial Epithelium:
792 Implications for Airway Inflammation in Cystic Fibrosis. *J Immunol*. 175:404–412.
793 doi:10.4049/jimmunol.175.1.404.
- 794 Mleczko, A.M., P. Celichowski, and K. Bąkowska-Żywicka. 2018. Transfer RNA-derived
795 fragments target and regulate ribosome-associated aminoacyl-transfer RNA
796 synthetases. *Biochimica et Biophysica Acta (BBA) - Gene Regulatory
797 Mechanisms*. 1861:647–656. doi:10.1016/j.bbagr.2018.06.001.
- 798 Moreau-Marquis, S., B. Coutermarsh, and B.A. Stanton. 2015. Combination of
799 hypothiocyanite and lactoferrin (ALX-109) enhances the ability of tobramycin and
800 aztreonam to eliminate *Pseudomonas aeruginosa* biofilms growing on cystic
801 fibrosis airway epithelial cells. *J Antimicrob Chemother*. 70:160–166.
802 doi:10.1093/jac/dku357.
- 803 Moss, R.B. 2002. Long-term Benefits of Inhaled Tobramycin in Adolescent Patients
804 With Cystic Fibrosis. *Chest*. 121:55–63. doi:10.1378/chest.121.1.55.
- 805 Nelson, M.T., D.J. Wolter, A. Eng, E.J. Weiss, A.T. Vo, M.J. Brittnacher, H.S. Hayden,
806 S. Ravishankar, G. Bautista, A. Ratjen, M. Blackledge, S. McNamara, L. Nay, C.
807 Majors, S.I. Miller, E. Borenstein, R.H. Simon, J.J. LiPuma, and L.R. Hoffman.
808 2020. Maintenance tobramycin primarily affects untargeted bacteria in the CF
809 sputum microbiome. *Thorax*. 75:780–790. doi:10.1136/thoraxjnl-2019-214187.
- 810 Novosad, S.A., and A.F. Barker. 2013. Chronic obstructive pulmonary disease and
811 bronchiectasis: *Current Opinion in Pulmonary Medicine*. 19:133–139.
812 doi:10.1097/MCP.0b013e32835d8312.

- 813 Ogawa, T., K. Takahashi, W. Ishida, T. Aono, M. Hidaka, T. Terada, and H. Masaki.
814 2020. Substrate recognition mechanism of tRNA-targeting ribonuclease, colicin
815 D, and an insight into tRNA cleavage-mediated translation impairment. *RNA*
816 *Biology*. 0:1–13. doi:10.1080/15476286.2020.1838782.
- 817 Parker, D., D. Ahn, T. Cohen, and A. Prince. 2016. Innate Immune Signaling Activated
818 by MDR Bacteria in the Airway. *Physiological Reviews*. 96:19–53.
819 doi:10.1152/physrev.00009.2015.
- 820 R Core Team. 2021. R: A Language and Environment for Statistical Computing. R
821 Foundation for Statistical Computing, Vienna, Austria.
- 822 Ramsey, B.W., M.S. Pepe, J.M. Quan, K.L. Otto, A.B. Montgomery, J. Williams-Warren,
823 M. Vasiljev-K, D. Borowitz, C.M. Bowman, B.C. Marshall, S. Marshall, and A.L.
824 Smith. 1999. Intermittent Administration of Inhaled Tobramycin in Patients with
825 Cystic Fibrosis. *N Engl J Med*. 340:23–30. doi:10.1056/NEJM199901073400104.
- 826 Randell, S.H., M.L. Fulcher, W. O’Neal, and J.C. Olsen. 2011. Primary Epithelial Cell
827 Models for Cystic Fibrosis Research. *In Cystic Fibrosis: Diagnosis and Protocols*,
828 Volume II: Methods and Resources to Understand Cystic Fibrosis. M.D. Amaral
829 and K. Kunzelmann, editors. Humana Press, Totowa, NJ. 285–310.
- 830 Ren, B., X. Wang, J. Duan, and J. Ma. 2019. Rhizobial tRNA-derived small RNAs are
831 signal molecules regulating plant nodulation. *Science*. 365:919–922.
832 doi:10.1126/science.aav8907.
- 833 Robinson, M.D., D.J. McCarthy, and G.K. Smyth. 2010. edgeR: a Bioconductor package
834 for differential expression analysis of digital gene expression data.
835 *Bioinformatics*. 26:139–140. doi:10.1093/bioinformatics/btp616.
- 836 Robinson, T.E., A.N. Leung, X. Chen, R.B. Moss, and M.J. Emond. 2009. Cystic fibrosis
837 HRCT scores correlate strongly with *Pseudomonas* infection. *Pediatric*
838 *Pulmonology*. 44:1107–1117. doi:10.1002/ppul.21107.
- 839 Roesch, E.A., D.P. Nichols, and J.F. Chmiel. 2018. Inflammation in cystic fibrosis: An
840 update. *Pediatric Pulmonology*. 53:S30–S50. doi:10.1002/ppul.24129.
- 841 Sagel, S.D., R. Kapsner, I. Osberg, M.K. Sontag, and F.J. Accurso. 2001. Airway
842 Inflammation in Children with Cystic Fibrosis and Healthy Children Assessed by
843 Sputum Induction. *Am J Respir Crit Care Med*. 164:1425–1431.
844 doi:10.1164/ajrccm.164.8.2104075.
- 845 Sagel, S.D., M.K. Sontag, J.S. Wagener, R.K. Kapsner, I. Osberg, and F.J. Accurso.
846 2002. Induced sputum inflammatory measures correlate with lung function in
847 children with cystic fibrosis. *The Journal of Pediatrics*. 141:811–817.
848 doi:10.1067/mpd.2002.129847.

- 849 Saks, M.E., and J.S. Conery. 2007. Anticodon-dependent conservation of bacterial
850 tRNA gene sequences. *RNA*. 13:651–660. doi:10.1261/rna.345907.
- 851 Sawicki, G.S., J.E. Signorovitch, J. Zhang, D. Latremouille-Viau, M. von Wartburg, E.Q.
852 Wu, and L. Shi. 2012. Reduced mortality in cystic fibrosis patients treated with
853 tobramycin inhalation solution. *Pediatr Pulmonol*. 47:44–52.
854 doi:10.1002/ppul.21521.
- 855 Schifano, J.M., J.W. Cruz, I.O. Vvedenskaya, R. Edifor, M. Ouyang, R.N. Husson, B.E.
856 Nickels, and N.A. Woychik. 2016. tRNA is a new target for cleavage by a MazF
857 toxin. *Nucleic Acids Research*. 44:1256–1270. doi:10.1093/nar/gkv1370.
- 858 Sethi, S. 2010. Infection as a comorbidity of COPD. *European Respiratory Journal*.
859 35:1209–1215. doi:10.1183/09031936.00081409.
- 860 Shanks, R.M.Q., N.C. Caiazza, S.M. Hinsa, C.M. Toutain, and G.A. O’Toole. 2006.
861 *Saccharomyces cerevisiae* -Based Molecular Tool Kit for Manipulation of Genes
862 from Gram-Negative Bacteria. *Appl Environ Microbiol*. 72:5027–5036.
863 doi:10.1128/AEM.00682-06.
- 864 Stanton, B.A. 2017. Effects of *Pseudomonas aeruginosa* CFTR chloride secretion
865 and the host immune response. *Am J Physiol Cell Physiol*. 312:C357–C366.
866 doi:10.1152/ajpcell.00373.2016.
- 867 Stoltz, D.A., D.K. Meyerholz, and M.J. Welsh. 2015. Origins of Cystic Fibrosis Lung
868 Disease. *N Engl J Med*. 372:351–362. doi:10.1056/NEJMra1300109.
- 869 Su, Z., B. Wilson, P. Kumar, and A. Dutta. 2020. Noncanonical Roles of tRNAs: tRNA
870 Fragments and Beyond. *Annual Review of Genetics*. 54:47–69.
871 doi:10.1146/annurev-genet-022620-101840.
- 872 Tao, E.-W., W.Y. Cheng, W.-L. Li, J. Yu, and Q.-Y. Gao. 2020. tiRNAs: A novel class of
873 small noncoding RNAs that helps cells respond to stressors and plays roles in
874 cancer progression. *Journal of Cellular Physiology*. 235:683–690.
875 doi:10.1002/jcp.29057.
- 876 Thompson, D.M., C. Lu, P.J. Green, and R. Parker. 2008. tRNA cleavage is a
877 conserved response to oxidative stress in eukaryotes. *RNA*. 14:2095–2103.
878 doi:10.1261/rna.1232808.
- 879 Tomita, K., T. Ogawa, T. Uozumi, K. Watanabe, and H. Masaki. 2000. A cytotoxic
880 ribonuclease which specifically cleaves four isoaccepting arginine tRNAs at their
881 anticodon loops. *PNAS*. 97:8278–8283. doi:10.1073/pnas.140213797.
- 882 Van Nostrand, E.L., G.A. Pratt, A.A. Shishkin, C. Gelboin-Burkhart, M.Y. Fang, B.
883 Sundararaman, S.M. Blue, T.B. Nguyen, C. Surka, K. Elkins, R. Stanton, F. Rigo,
884 M. Guttman, and G.W. Yeo. 2016. Robust transcriptome-wide discovery of RNA

- 885 binding protein binding sites with enhanced CLIP (eCLIP). *Nat Methods*. 13:508–
886 514. doi:10.1038/nmeth.3810.
- 887 Vij, N., S. Mazur, and P.L. Zeitlin. 2009. CFTR Is a Negative Regulator of NFκB
888 Mediated Innate Immune Response. *PLOS ONE*. 4:e4664.
889 doi:10.1371/journal.pone.0004664.
- 890 Wickham, H. 2016. ggplot2: Elegant Graphics for Data Analysis. Springer-Verlag New
891 York.
- 892 Williams, B.J., J. DehnboſTEL, and T.S. Blackwell. 2010. *Pseudomonas aeruginosa*:
893 Host defence in lung diseases. *Respirology*. 15:1037–1056. doi:10.1111/j.1440-
894 1843.2010.01819.x.
- 895 Winther, K., J.J. Tree, D. Tollervey, and K. Gerdes. 2016. VapCs of *Mycobacterium*
896 *tuberculosis* cleave RNAs essential for translation. *Nucleic Acids Research*.
897 44:9860–9871. doi:10.1093/nar/gkw781.
- 898 Yi, B., A.H. Dalpke, and S. Boutin. 2021. Changes in the Cystic Fibrosis Airway
899 Microbiome in Response to CFTR Modulator Therapy. *Front. Cell. Infect.*
900 *Microbiol.* 11. doi:10.3389/fcimb.2021.548613.
- 901 Yu, Q., E.F. Griffin, S. Moreau-Marquis, J.D. Schwartzman, B.A. Stanton, and G.A.
902 O’Toole. 2012. In vitro evaluation of tobramycin and aztreonam versus
903 *Pseudomonas aeruginosa* biofilms on cystic fibrosis-derived human airway
904 epithelial cells. *J Antimicrob Chemother.* 67:2673–2681. doi:10.1093/jac/dks296.
- 905 Zhang, H., Y. Zhang, Z. Song, R. Li, H. Ruan, Q. Liu, and X. Huang. 2020. sncRNAs
906 packaged by *Helicobacter pylori* outer membrane vesicles attenuate IL-8
907 secretion in human cells. *International Journal of Medical Microbiology*.
908 310:151356. doi:10.1016/j.ijmm.2019.151356.
- 909

910 **Figures**



911 **Figure 1. Tobramycin reduces the ability of OMVs secreted by *P. aeruginosa* to stimulate**

912 **IL-8 secretion by CF-HBECs. (A)** A schematic diagram shows the experimental design. **(B)**

913 Growth curve (in microtiter plates) of PA14 in LB alone (PA14) or in LB with tobramycin (1

914 $\mu\text{g}/\text{mL}$; PA14+Tobi). Lines represent the averages from three biological replicates, and error

915 bars indicate standard error of means (SEM). The presence of tobramycin inhibited PA14

916 growth by 33% between the 13 to 20 hour time points. **(C)** OMV concentration of purified ctrl-

917 OMVs and Tobi-OMVs ($n = 12$) measured with nanoparticle tracking analysis (Nanosight

918 NS300). The red line connects the mean concentration of the two groups and demonstrates a

919 38% increase in Tobi-OMVs concentration compared to ctrl-OMVs concentration. Data are

920 shown as the means \pm SEM **(D)** Primary CF-HBECs from three donors ($n = 3$) were polarized in

921 ALI culture before being exposed to either the same number of ctrl-OMVs or Tobi-OMVs or 40%

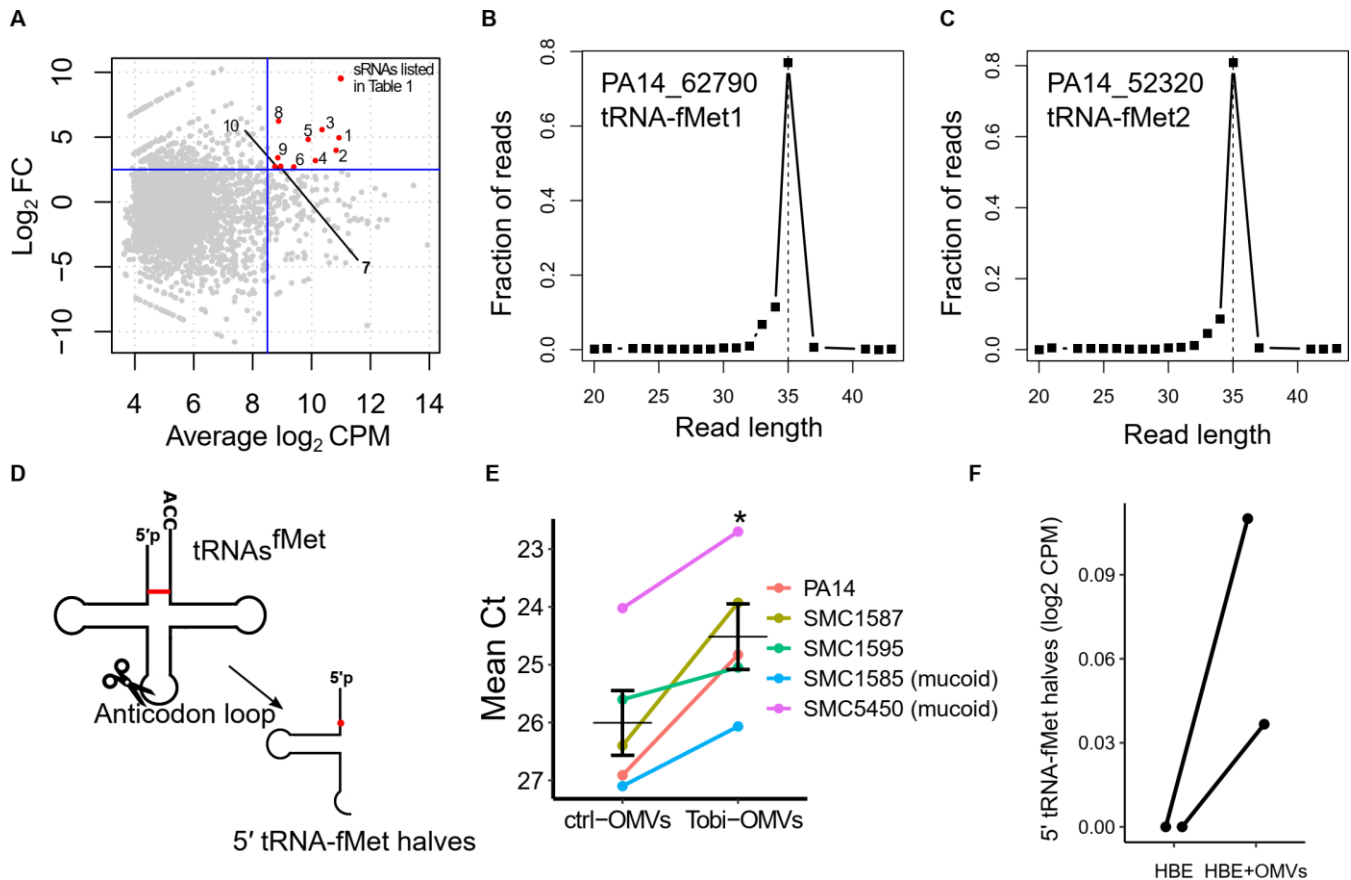
922 more Tobi-OMVs (1.4X Tobi-OMVs) for 6 hours. The basolateral medium was collected to

923 measure IL-8. Lines connect experiments conducted with CF-HBECs from the same donor.

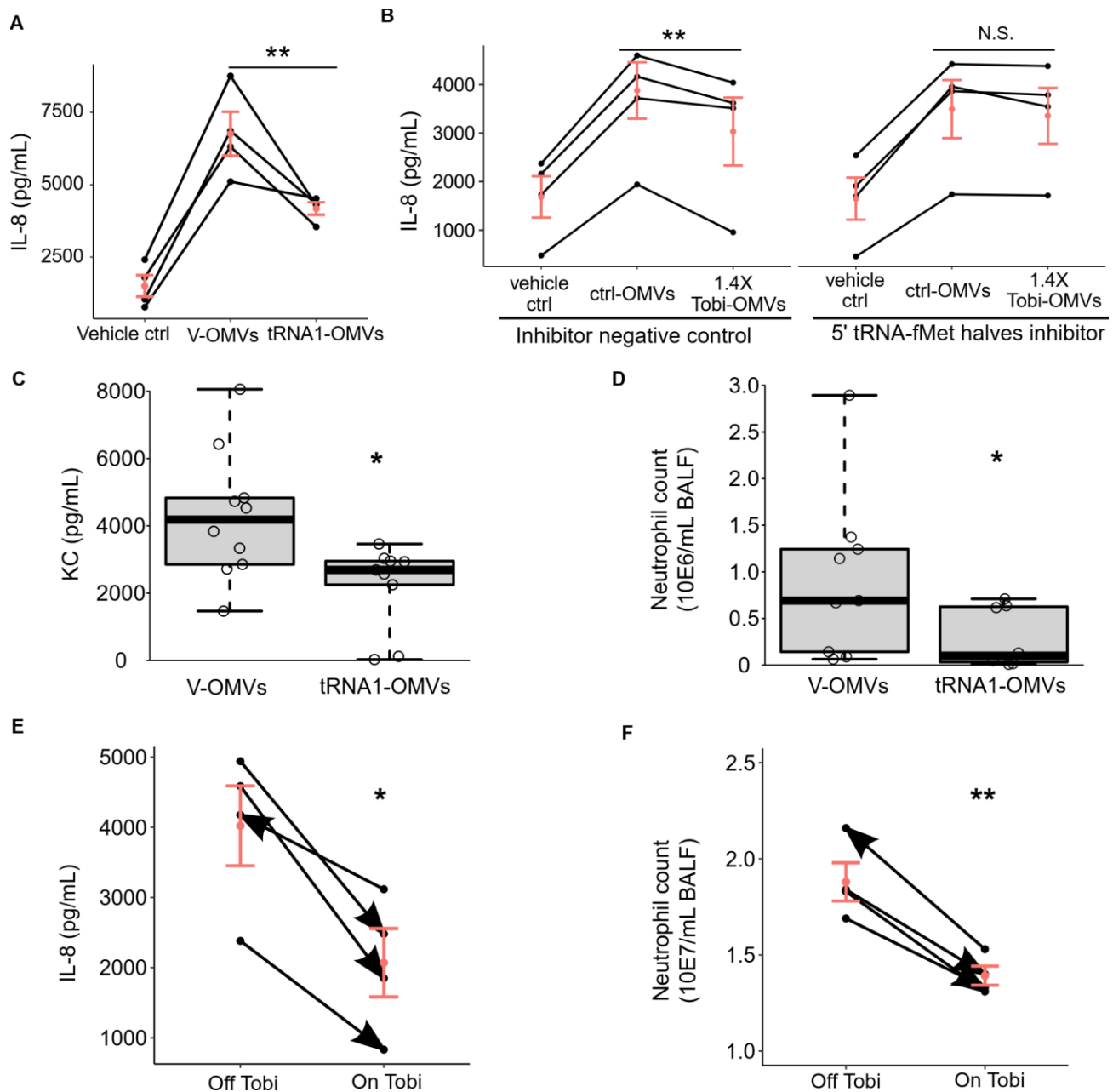
924 Horizontal red lines and red dots indicate means \pm SEM. Paired t-tests **(C)**; Linear mixed-effects

925 models with CF-HBEC donor as a random effect were used to calculate P values **(D)**; * $P < 0.05$;

926 ** $P < 0.01$; *** $P < 0.001$.

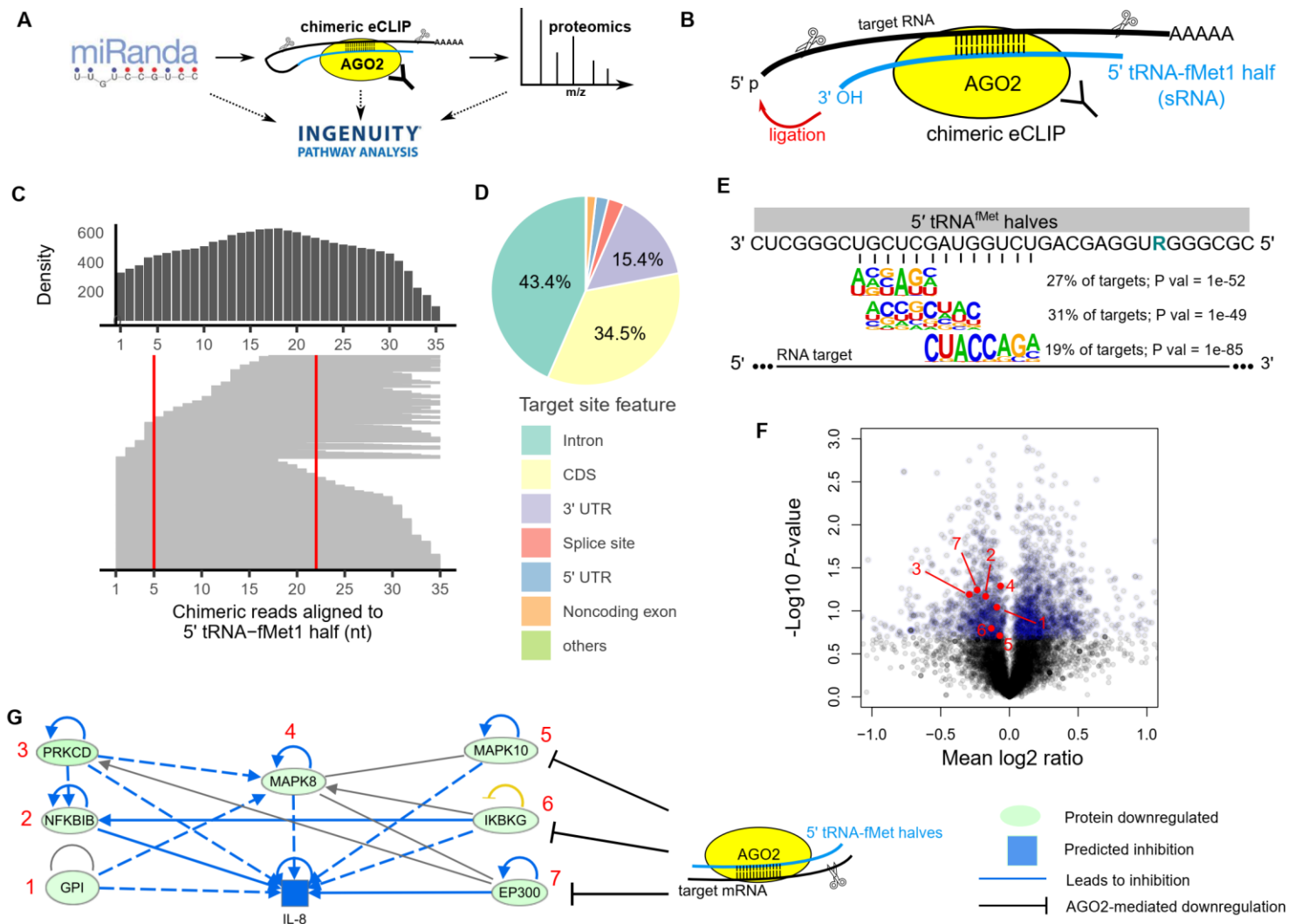


927 **Figure. 2 Tobramycin increases the abundance of 5' tRNA-fMet halves in OMVs, and the**
 928 **tRNA halves are transferred into host cells. (A)** MA plot comparing the small RNA
 929 expression profile in Tobi-OMVs and ctrl-OMVs ($n = 3$ for each group). Each dot represents a
 930 unique sequence read. The most abundant and most induced PA14 sRNAs by tobramycin treatment
 931 are highlighted in red and listed in Table 1. **(B and C)** Length distribution of Tobi-OMVs sRNAs
 932 mapped to gene locus PA14_62790 **(B)** and PA14_52320 **(C)**. **(D)** Secondary cloverleaf
 933 structure of tRNA^{fMet} and cleavage site in the anticodon loop to generate 5' tRNA-fMet halves.
 934 The red line indicates the only different pair of nucleotides between the two tRNA^{fMet}, and the
 935 red dot represents the only nucleotide difference between the two 5' tRNA-fMet halves. **(E)**
 936 qPCR for 5' tRNA-fMet halves in ctrl-OMVs and Tobi-OMVs purified from PA14 and four clinical
 937 isolates ($n = 5$ strains), including two mucooid and two non-mucooid strains. The qPCR primers
 938 and probe were designed to detect both 5' tRNA-fMet halves. Horizontal lines indicate means \pm
 939 SEM. A paired t-test was used to establish significance. * $P < 0.05$. **(F)** Both 5' tRNA-fMet
 940 halves were detected in polarized primary HBE cells exposed to ctrl-OMVs but not in unexposed
 941 cells using small RNA sequencing (from two donors; $n = 2$). Sequence reads in **(F)** are from our
 942 previously published dataset (Koeppen et al., 2016).



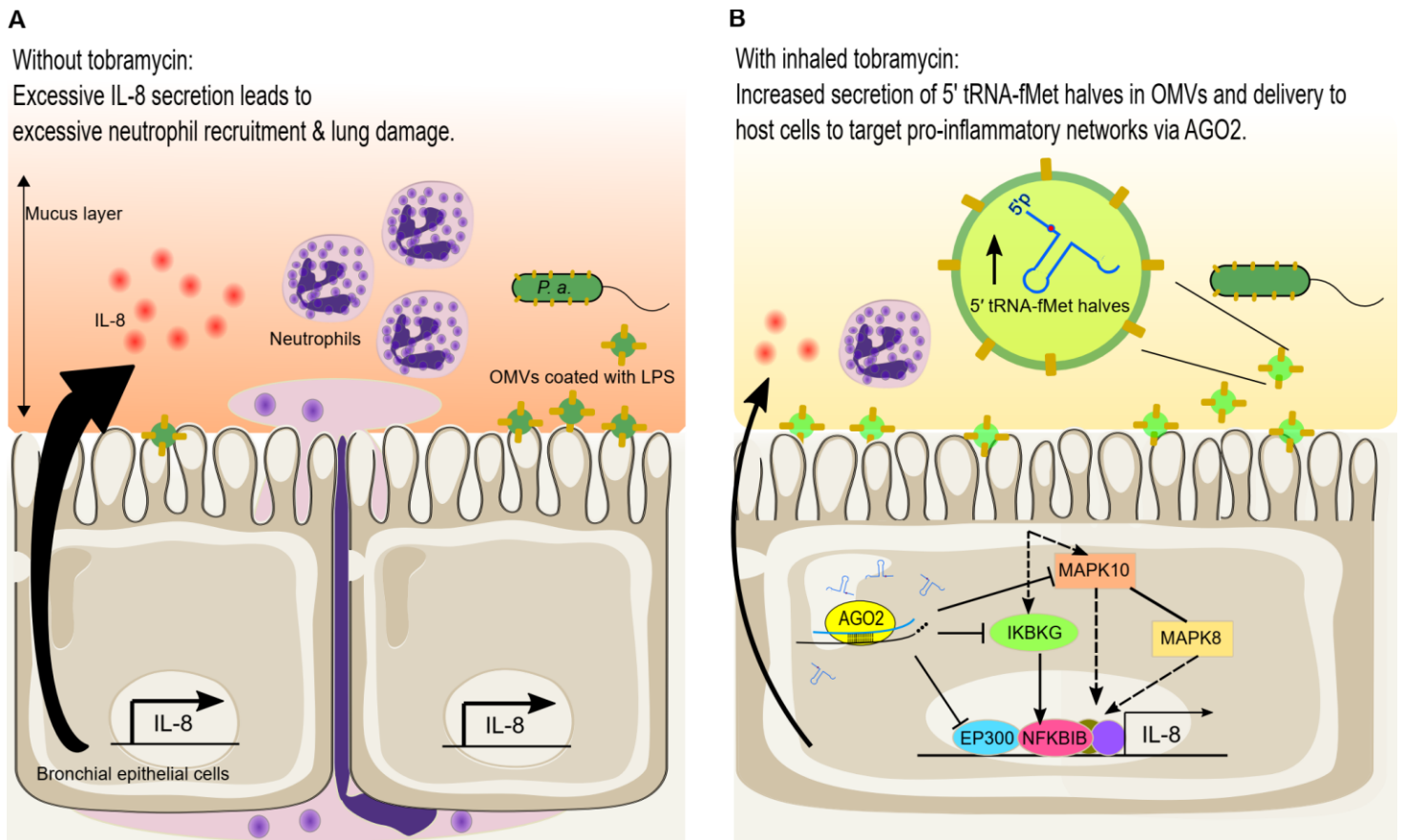
943 **Figure 3. 5' tRNA-fMet halves reduce IL-8 secretion *in vitro* and *in vivo*.** (A) Polarized CF-
 944 HBECs ($n = 4$) exposed to tRNA1-OMV secreted less IL-8 compared to cells exposed to V-
 945 OMV. (B) The Tobi-OMV effect of reducing IL-8 secretion was abolished by transfection of an
 946 antisense RNA oligo inhibitor that anneals to both 5' tRNA-fMet halves (5' tRNA-fMet halves
 947 inhibitor) but not by transfection of a negative control inhibitor ($n= 4$). Lines in panels A and B
 948 connect data points using the cells from the same donor, a biological replicate. A linear mixed-
 949 effects model with CF-HBEC donor as a random effect was used to calculate P values. (C and

950 **D)** BALF from mice exposed to V-OMVs or tRNA1-OMVs was collected to measure KC
951 concentration (**C**) and neutrophil number (**D**). Minimum-to-maximum whisker and box plots
952 showing the median and interquartile ranges. 9 to 10 mice were used per group, and Wilcoxon
953 rank-sum tests were used to test significance. (**E** and **F**) BALF samples collected from four CF
954 subjects ($n= 4$) during the 4-week administration of inhaled tobramycin (On Tob) or not (Off
955 Tob) with BALF IL-8 levels in panel (**E**) and BALF neutrophil content in panel (**F**). Lines connect
956 data points from the same subject, and the arrowheads indicate the sample collection order for
957 each CF subject. Linear mixed-effect models were used to account for donor-to-donor variability
958 and the number of days between collection dates for each sample pair (Supplemental Table 1).
959 Horizontal red lines and red dots indicate means \pm SEM; N.S., not significant; * $P < 0.05$; ** $P <$
960 0.001.



961 **Figure 4. 5' tRNA-fMet halves downregulate protein expression in a sequence-specific**
 962 **manner mediated by AGO2.** (A) Schematic representation of the three-step approach to
 963 identify targets of 5' tRNA-fMet halves leading to differential protein expression. (B) Diagram of
 964 chimeric eCLIP to identify RNAs pulled down with AGO2. Samples were treated with RNase I
 965 for RNA fragmentation followed by immunoprecipitation of AGO2-mRNA-sRNA complexes
 966 before mRNA-sRNA ligation to generate chimeric reads. (C) Alignment of chimeric reads to the
 967 5' tRNA-fMet1 half sequence and the count distribution of each nucleotide (top density plot).
 968 Chimeric reads were identified in tRNA-fMet1 half-transfected CF-HBECs (one donor; $n = 1$)
 969 and contained at least 18-nt long 5' tRNA-fMet1 half subsequences. The red lines indicate the
 970 region where the primer performs targeted chimeric eCLIP anneals. (D) Distribution of target

971 site features identified with the targeted chimeric eCLIP. **(E)** Sequence logos of most significant
972 enriched target RNA motifs and the complementary sequence of 5' tRNA-fMet halves. R
973 denotes a purine nucleotide (G/A). **(F)** Volcano plot of proteomic analysis of polarized CF-
974 HBECs (three donors; $n = 3$) treated with tRNA1-OMVs compared to cells treated with V-OMVs.
975 The top 20% differentially expressed proteins, determined by paired t-tests, are colored in blue.
976 Red dots with numbers represent down-regulated proteins corresponding to proteins numbered
977 in panel (G). **(G)** IPA identified a down-regulated pro-inflammatory network in the five
978 consensus pathways (table 2), leading to decreased IL-8 expression. mRNA transcripts
979 encoding MAPK10, IKBKG, and EP300 were identified as binding targets of tRNA-fMet1 half in
980 the targeted chimeric eCLIP experiment.



981 **Figure 5. Graphical abstract indicating the anti-inflammatory effect of tobramycin**

982 **mediated by 5' tRNA-fMet halves in *P. aeruginosa* OMVs. (A) *P. aeruginosa* colonizes the**

983 CF lungs and secretes OMVs. OMVs diffuse through the mucus layer overlying bronchial

984 epithelial cells and induce IL-8 secretion, which recruits excessive neutrophils and causes lung

985 damage. (B) Tobramycin increases 5' tRNA-fMet halves in OMVs secreted by *P. aeruginosa*. 5'

986 tRNA-fMet halves are delivered into host cells and loaded into the AGO2 protein complex to

987 down-regulate protein expression of MAPK10, IKBKG, and EP300, which suppresses OMV-

988 induced IL-8 secretion and neutrophil recruitment. A reduction in neutrophils in BALF is

989 predicted to improve lung function and decrease lung damage.

990 **Tables**

991 **Table 1. Top 10 most abundant and most differentially induced sRNAs in Tobi-OMVs**
992 **compared to ctrl-OMVs**

| # | PA14 locus | Gene product of the locus | Log2FC | Average Log2CPM | length | Minimum free energy (kcal/mol) ^A |
|----|------------|---------------------------|--------|-----------------|--------------------------|---|
| 1 | Multiple | tRNA-Asp | 4.95 | 10.93 | 23 (20, 23) ^B | -0.2 |
| 2 | Multiple | 16S rRNA | 3.98 | 10.83 | 33 (30-39) ^B | -6.9 |
| 3 | Multiple | 23S rRNA | 5.57 | 10.35 | 44 | -14.6 |
| 4 | Multiple | tRNA-Ala | 3.19 | 10.13 | 34 | -8 |
| 5 | 62790 | tRNA-fMet1 | 4.82 | 9.88 | 35 | -7.5 |
| 6 | 28740 | tRNA-Pro | 2.70 | 9.39 | 36 | -9.7 |
| 7 | 52320 | tRNA-fMet2 | 2.74 | 8.95 | 35 | -9.3 |
| 8 | 61760 | tRNA-Gln | 6.23 | 8.88 | 20 | -0.2 |
| 9 | 30720 | tRNA-Cys | 3.41 | 8.85 | 40 | -4.6 |
| 10 | multiple | 5S rRNA | 2.72 | 8.75 | 45 | -3.8 |

993 ^AThe minimum free energy for each sRNA was predicted using the RNAfold web server (Gruber
994 et al., 2008)

995 ^BMultiple reads of different lengths were mapped to the same locus, and the most abundant
996 read is listed in Table 1 and Figure 2A.

997 **Table 2. The consensus of significantly enriched signaling pathways identified using**
 998 **three approaches^A.**

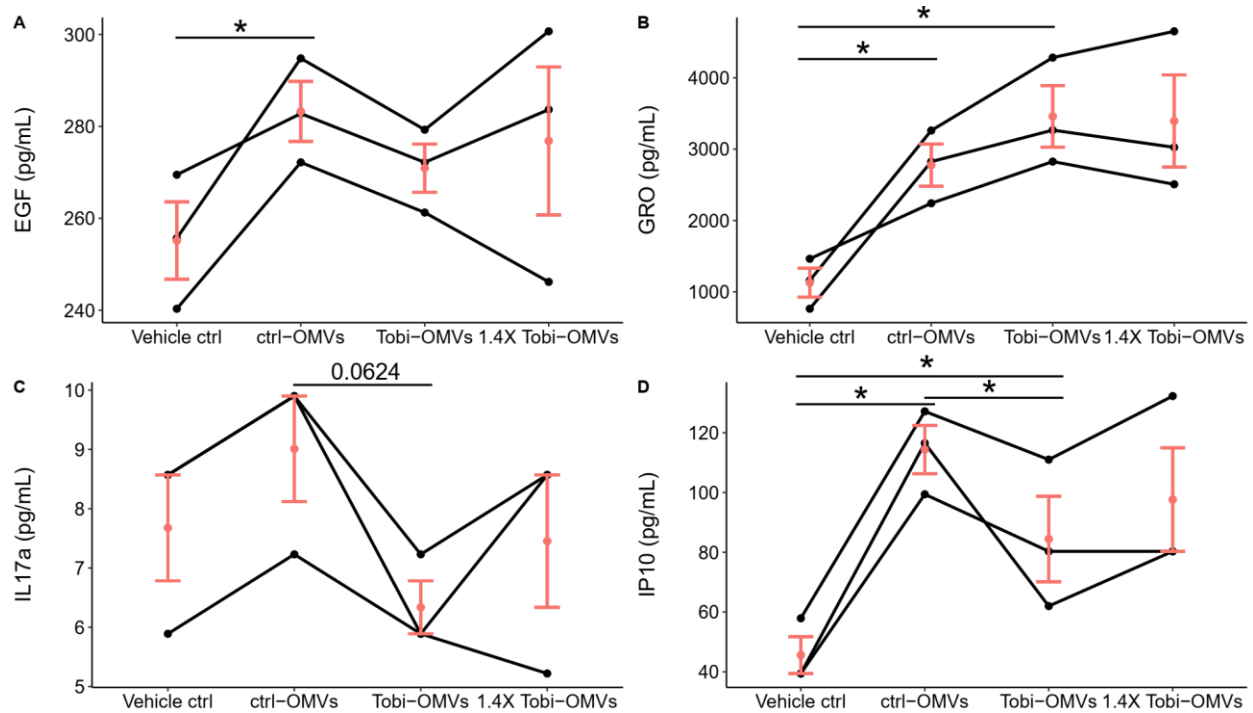
| Canonical pathway | Gene target prediction | | Gene target validation | | Protein expression | |
|---|-----------------------------|----------------------|------------------------------------|----------------------|--------------------------------|----------------------|
| | <i>P</i> value | z-score ^C | <i>P</i> value | z-score ^C | <i>P</i> value | z-score ^C |
| | miRanda (1518) ^B | | chimeric eCLIP (1936) ^B | | Proteomics (2168) ^B | |
| Integrin-linked kinase (ILK) Signaling | 0.0005 | -3.26 | 0.0041 | -0.53 | 1.1E-08 | -2.27 |
| LPS-stimulated MAPK Signaling | 0.0087 | -3.46 | 0.0005 | -3.60 | 7.7E-05 | -0.68 |
| HIF1a Signaling | 0.0022 | -3 | 0.0072 | -4.35 | 0.0015 | -0.87 |
| IL-17A Signaling in Airway Cells | 0.0011 | -2.53 | 0.0085 | -1.66 | 0.0077 | -0.30 |
| IL-6 Signaling | 0.0002 | -4.02 | 0.0389 | -3.46 | 0.0141 | -0.94 |

999 ^A There are 38 consensus pathways. Only consensus pathways predicted to downregulate IL-8
 1000 secretion in epithelial cells by IPA are listed.

1001 ^B Number in parentheses indicates the number of genes/proteins used to perform pathway
 1002 enrichment analysis.

1003 ^C Negative z-scores indicate that the pathways are predicted to be down-regulated.

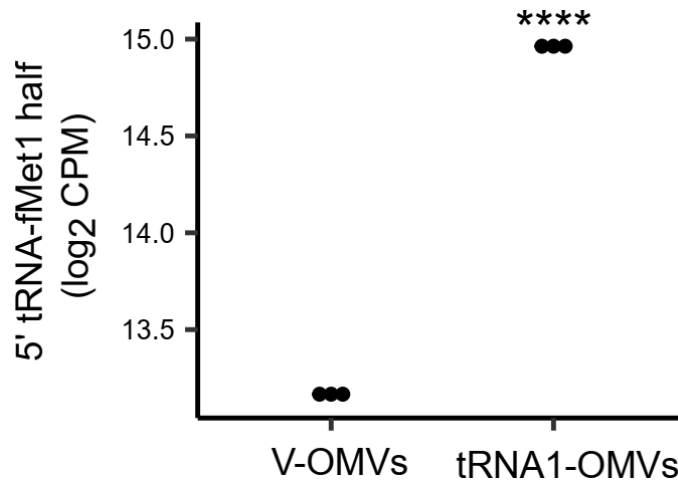
1004



1005

1006 **Supplemental Figure 1. OMV effects on EGF, GRO, IL17a, and IP10.** CF-HBECs from three
1007 donors ($n = 3$) were polarized in ALI culture before being exposed to either the same number of
1008 ctrl-OMVs, Tobi-OMVs, or 40% more Tobi-OMVs (1.4X Tobi-OMVs). After six-hour exposure,
1009 the basolateral medium was collected and diluted 4-fold for 41-plex measurements. Cytokines
1010 other than IL-8, EGF, GRO, IL17a, and IP10 were below the detection limit. Lines connect
1011 experiments conducted with CF-HBECs from the same donor. Horizontal red lines and red dots
1012 indicate means \pm SEM. Linear mixed-effects models with CF-HBEC donor as a random effect
1013 were used to calculate P values; $*P < 0.05$.

1014



1015

1016 **Supplemental Figure 2. 5' tRNA-fMet1 half is over-expressed in tRNA1-OMVs compared**

1017 **to V-OMVs.** Small RNAs in V-OMVs and tRNA1-OMVs harvested from LB culture with

1018 arabinose were subjected to small RNA sequencing to quantify 5' tRNA-fMet1 half ($n = 3$). ****

1019 FDR < 0.0001.

1020

1021 **Supplemental Table 1. BALF sample collection dates**

| Subject | TOBI | Sample collection date | # of Days apart^A |
|----------------|-------------|-------------------------------|------------------------------------|
| A | Off | 4/26/2017 | 0 |
| A | On | 3/28/2018 | 336 |
| B | Off | 3/7/2018 | 0 |
| B | On | 8/29/2018 | 175 |
| C | Off | 4/1/2015 | 791 |
| C | On | 1/30/2013 | 0 |
| D | Off | 6/14/2017 | 0 |
| D | On | 6/27/2018 | 378 |

1022 ^AFor each pair of samples, the earlier collection date is marked as day 0.